iScience

CellPress
OPEN ACCESS

Article

AXL Is a Driver of Stemness in Normal Mammary Gland and Breast Cancer

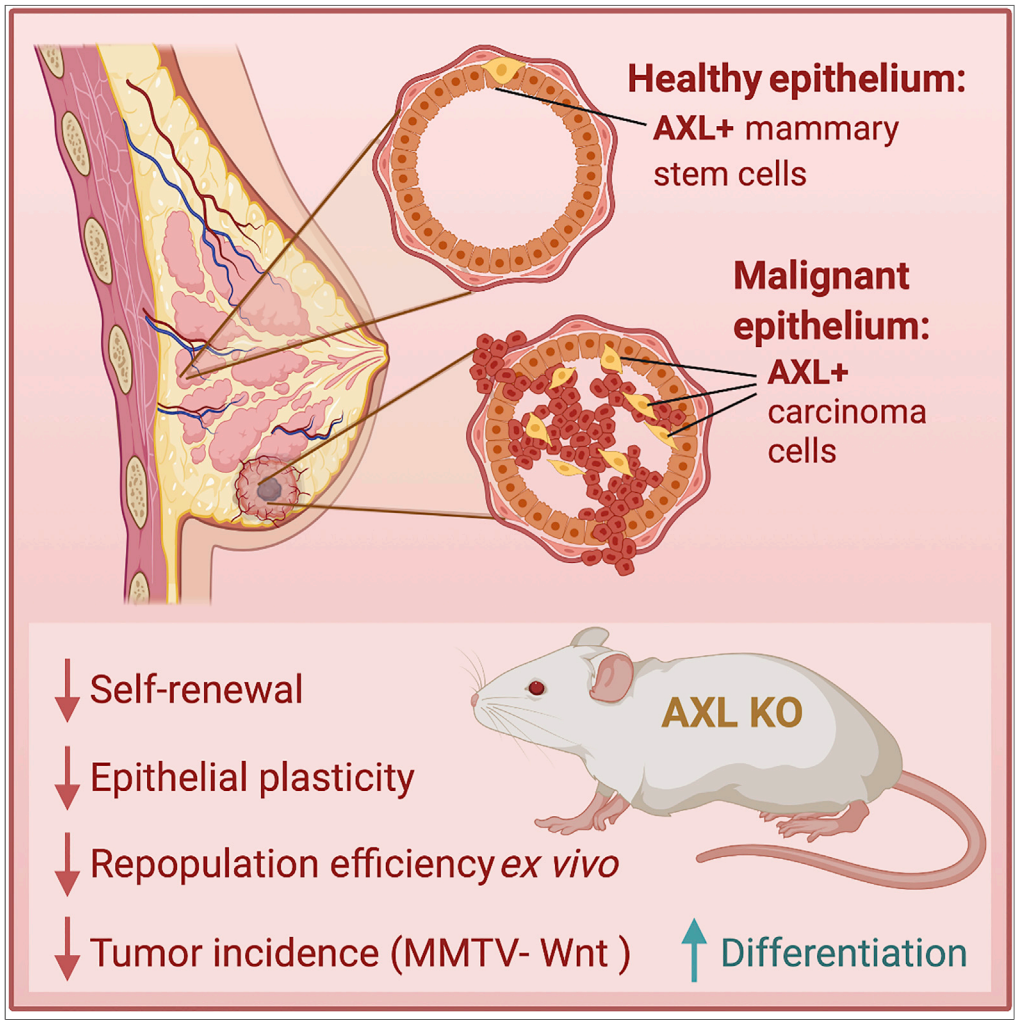

Agnete S.T. Engelsen, Katarzyna Wnuk-Lipinska, Sebastien Bougnaud, ..., Ole W. Petersen, Mark A. LaBarge, James B. Lorens

mlabarge@coh.org (M.A.L.)
jim.lorens@uib.no (J.B.L.)

HIGHLIGHTS

AXL + mammary epithelial cells have multipotent activity conserved in women and mice

AXL allows accesses to epithelial-to-mesenchymal transition genes and prevents differentiation into luminal cells

Deletion of *Axl* reduced incidence of *Wnt1*-driven tumors in mice

Provides a rationale explaining the advantage to cancer cells that co-opt AXL signaling

Engelsen et al., iScience *23*, 101649
November 20, 2020
https://doi.org/10.1016/j.isci.2020.101649

iScience

CellPress
OPEN ACCESS

Article

AXL Is a Driver of Stemness in Normal Mammary Gland and Breast Cancer

Agnete S.T. Engelsen,[1,3,4,17] Katarzyna Wnuk-Lipinska,[1,17] Sebastien Bougnaud,[1,3] Fanny A. Pelissier Vatter,[1,3] Crina Tiron,[1] René Villadsen,[5] Masaru Miyano,[8,16] Maria L. Lotsberg,[1,3] Noëlly Madeleine,[1] Pouda Panahandeh,[1] Sushil Dhakal,[1] Tuan Zea Tan,[13] Stacey D'mello Peters,[1] Sturla Grøndal,[1] Sura M. Aziz,[2,3,9] Silje Nord,[10] Lars Herfindal,[1] Martha R. Stampfer,[8] Therese Sørlie,[10] Rolf A. Brekken,[11] Oddbjørn Straume,[3,12] Nils Halberg,[1] Gro Gausdal,[1] Jean Paul Thiery,[3,4,7,13,14,15] Lars A. Akslen,[2,3,9] Ole W. Petersen,[5,6] Mark A. LaBarge,[3,8,16,*] and James B. Lorens[1,3,18,*]

SUMMARY

The receptor tyrosine kinase AXL is associated with epithelial plasticity in several solid tumors including breast cancer and AXL-targeting agents are currently in clinical trials. We hypothesized that AXL is a driver of stemness traits in cancer by co-option of a regulatory function normally reserved for stem cells. AXL-expressing cells in human mammary epithelial ducts co-expressed markers associated with multipotency, and AXL inhibition abolished colony formation and self-maintenance activities while promoting terminal differentiation *in vitro*. *Axl*-null mice did not exhibit a strong developmental phenotype, but enrichment of *Axl*$^{+}$ cells was required for mouse mammary gland reconstitution upon transplantation, and *Axl*-null mice had reduced incidence of *Wnt1*-driven mammary tumors. An AXL-dependent gene signature is a feature of transcriptomes in basal breast cancers and reduced patient survival irrespective of subtype. Our interpretation is that AXL regulates access to epithelial plasticity programs in MaSCs and, when co-opted, maintains acquired stemness in breast cancer cells.

INTRODUCTION

Phenotypic plasticity, the capacity of a single genotype to exhibit variable phenotypes in different environments, is a key feature of epithelial homeostasis. The multi-lineage potential of epithelial stem cells is thought to be maintained by specific niche microenvironments and elicited by regenerative cues from tissue wounding and inflammation (Blanpain and Fuchs, 2014). Co-option of these homeostatic mechanisms by carcinoma cells facilitates transition between stem-like mesenchymal and differentiated epithelial states in response to tumor microenvironment dynamics and therapeutic challenge and is associated with poor clinical outcome (Nieto et al., 2016).

The adult human mammary gland is a bilayer epithelium with basal-located myoepithelial (MEP) cells that surround luminal epithelial cells (LEPs) that are thought to be maintained by mammary stem cells (MaSCs), which continue to elude a consensus definition (Fridriksdottir et al., 2017; Petersen and Polyak, 2010; Villadsen et al., 2007; Eirew et al., 2008). The breast epithelium exhibits remarkable organ-scale remodeling during puberty and multiple lactation cycles that requires a renewable reservoir of stem and committed progenitor cells (Visvader and Stingl, 2014). Stem cell-related gene expression programs are utilized by breast cancer cells during malignant progression – here also referred to as co-option (Lawson et al., 2015; Billaud and Santoro, 2011). Transcription factors (e.g. SNAI1/2) that regulate the epithelial-to-mesenchymal transition (EMT) gene program during early development influence MaSC state transitions, and their dysregulation causes luminal compartment expansion (Phillips et al., 2014; Ye et al., 2015). The AXL receptor tyrosine kinase (RTK) is associated with malignant progression and poor patient survival in several malignancies including breast cancer (Davidsen et al., 2017). AXL is activated by a single ligand, GAS6, that activates a unique RTK signaling network in cancer cells (Meyer et al., 2013). AXL expression is correlated with epithelial-mesenchymal transition, immune evasion, increased metastatic potential, as well as therapeutic resistance in several tumor types (Gjerdrum et al., 2010; Ludwig et al., 2018; Zhang et al., 2012;

[1]Department of Biomedicine, University of Bergen, 5021 Bergen, Norway

[2]Department of Clinical Science, University of Bergen, 5021 Bergen, Norway

[3]Centre for Cancer Biomarkers, University of Bergen, 5021 Bergen, Norway

[4]INSERM UMR 1186, Integrative Tumor Immunology and Genetic Oncology, Gustave Roussy Cancer Campus Grand Paris, 94800 Villejuif, France

[5]Department of Cellular and Molecular Medicine, University of Copenhagen, Copenhagen, Copenhagen N 2200, Denmark

[6]Novo Nordisk Foundation Center for Stem Cell Biology, University of Copenhagen, Copenhagen, Copenhagen N 2200, Denmark

[7]Cancer Science Institute of Singapore, National University of Singapore, Singapore 117599, Singapore

[8]Biolgical Systems and Engineering Division, Lawrence Berkeley National Laboratory, Berkeley, CA 94720, USA

[9]Department of Pathology, Haukeland University Hospital, 5021 Bergen, Norway

[10]Department of Cancer Research, Oslo University Hospital, 0310 Oslo, Norway

[11]Hamon Center for Therapeutic Oncology Research, UT Southwestern Medical Center, Dallas, TX 75390, USA

[12]Department of Oncology and Medical Physics, Haukeland University

Continued

Antony et al., 2016; Lotsberg et al., 2020; Terry et al., 2019). AXL is therefore an important therapeutic target, and AXL kinase inhibitors are currently in clinical trials (Davidsen et al., 2017).

In contrast to the prominence of AXL in cancer progression, the role of AXL signaling in normal physiology is comparatively unknown, limiting our understanding of the consequences of AXL activation in malignant progression. We hypothesize that AXL is a gatekeeper to the signaling cascades and gene programs that enable epithelial plasticity, and that its principle role in normal epithelia is to regulate access to programs that are permissive for stem or progenitor cell states. Herein we identify AXL as a conserved mediator that governs human and mouse MaSC activity, providing a conserved marker of adult stem cells that is correlated with epithelial plasticity.

RESULTS

AXL Expression Is a Feature of Rare Adult Human Breast Epithelial Cells

AXL knockout mice are viable and do not show a developmental phenotype (Lu and Lemke, 2001); thus there is no evidence linking AXL to developmental EMT. This prompted us to investigate whether AXL is a heretofore unappreciated feature of adult human mammary epithelia. Immunofluorescence staining for AXL expression in normal human breast tissue specimens detected infrequent AXL-expressing cells. A subset of the AXL-expressing cells in human mammary gland overlap with the K14/K19 double-positive population, a phenotype associated with multipotency (Shimono et al., 2009; Huo and Macara, 2014; Dravis et al., 2015; Lilja et al., 2018; Wuidart et al., 2018; Spike et al., 2012; Giraddi et al., 2018; Chen et al., 2017) (Figures 1A–1D). Small clusters of AXL^+ epithelial cells co-expressing of luminal (K19) and basal (K14) markers were also detected in lobular acini (Figures 1E–1H). In ductal structures, AXL-expressing cells represent a unique population of cells with strong AXL staining (Figure 1I). RNA *in situ* hybridization (RNA-ISH) analysis of the ductal structures verified this expression pattern (Figure 1J (*AXL*, brown)). Epithelial cells with >15 *AXL* mRNA transcripts comprised a minority of cells of the mammary epithelium, consistent with a low Histo-score of 63 (Figure 1L). In contrast, RNA-ISH for the AXL-ligand *GAS6* (Figure 1K), revealed a more widely distributed expression among most LEPs, and this heterogeneous expression pattern is correspondingly reflected in the higher Histo-score of 141 (Figure 1M). Dual RNA-ISH detected cells with *GAS6* transcripts in LEP that were adjacent to the *AXL*-expressing cells in the same FFPE tissue sections (Figure 1N; RNA-ISH controls are shown in Figure S1). Collectively, these results suggested that AXL-expressing cells constitute a rare population of cells in the mammary epithelium. Some of the weaker staining AXL-positive cells in the ductal and lobular epithelium are $K14^+/K19^+$ positive, and based on RNA-ISH the GAS6 ligand is produced mainly by luminal cells.

Phenotypic Characterization of AXL-Expressing Cells in Human Breast Epithelium

To further characterize the population of AXL^+ cells in mammary epithelia, we analyzed primary uncultured human mammary epithelial cells (HMECs) from reduction mammoplasty specimens by flow cytometry using AXL antibody in addition to a panel of LEP, MEP, and stem/progenitor cell markers: CD227, CD10, EPCAM, CD49f. AXL-expressing HMEC represented 1–6% of the total HMEC population from different individuals (n = 5), which partitioned into an $EPCAM^+/CD49f^+$ subpopulation that is discrete from differentiated LEP ($CD227^+/CD10^-$) and MEP ($CD227^-/CD10^+$) populations (Figures 2A–2D). The EPCAM/CD49f/CD227/CD10/AXL FACS-analyzed HMECs were evaluated by spanning-tree progression analysis of density-normalized events (SPADE) to generate a putative hierarchical tree. The SPADE technique organizes groups of similar cells next to each other based on expression similarity, creating tree-like structures. AXL expression was highest in the node located at the apex of separate LEP (CD227 biased) and MEP (CD49f biased) radiations (Figure 2E). Next, we evaluated the expression of AXL, KIT, K14, and K19, among 25 other proteins, in a 29-marker mass cytometry (CyTOF) data set derived from dissociated primary breast epithelia of 57 women (Pelissier Vatter et al., 2018). Non-linear dimensionality reduction by t-distributed stochastic neighbor embedding projection and unsupervised clustering of intra-lineage subpopulations identified distinct LEP, MEP, and progenitor cells (Figure 2F). This high-dimensional analysis showed that AXL was primarily associated with KIT/K14/K19 expressing progenitor cells (Figures 2G and 2H). Notably, K14 was expressed relatively more than K19, which is anecdotally consistent with our immunofluorescence observations that K19 exhibits consistently lower, yet detectable, expression. Previously EpCAM+/CD49f + epithelia that express K14 and K19, and shared properties of LEP and MEP, were shown to be enriched for multipotent activity in human mammary epithelia (Villadsen et al., 2007). Epithelial cells expressing KIT were shown to be enriched for multipotent epithelial cell activity (Garbe et al., 2012; Lim et al., 2009; Pelissier et al., 2014). The finding that AXL also is expressed in epithelial cells bearing this

Hospital, 5021 Bergen, Norway

[13]Department of Biochemistry, Yong Loo Lin School of Medicine, National University of Singapore, Singapore 119228, Singapore

[14]Institute of Molecular and Cell Biology, Agency for Science, Technology and Research, A-STAR, Singapore 138673, Singapore

[15]Bioland Laboratory, Guangzhou Regenerative Medicine and Health, Bio-island, Guangzhou, 510320, China

[16]Department of Population Sciences, Beckman Research Institute at City of Hope, Duarte, CA 91910, USA

[17]These authors contributed equally

[18]Lead Contact

*Correspondence: mlabarge@coh.org (M.A.L.), jim.lorens@uib.no (J.B.L.)

https://doi.org/10.1016/j.isci.2020.101649

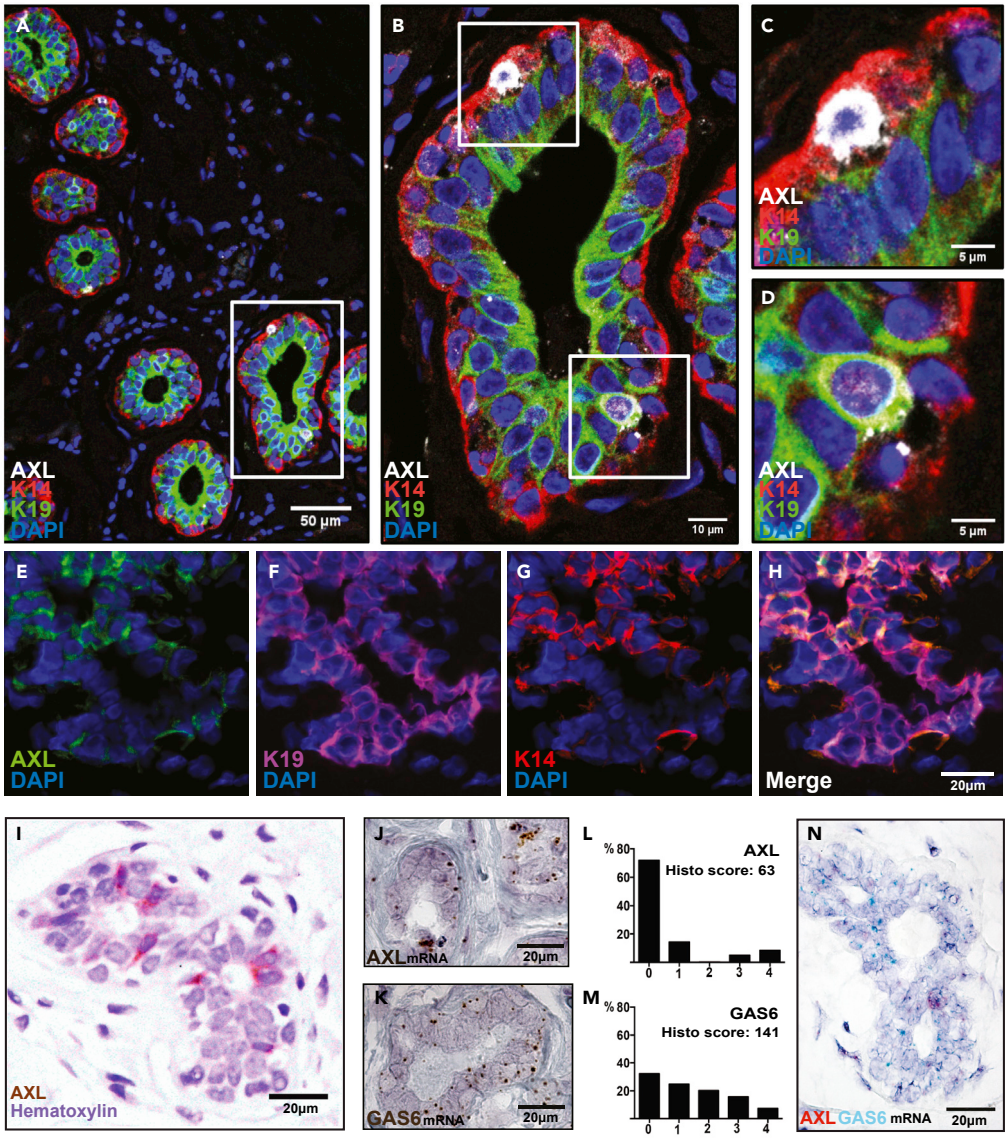

Figure 1. AXL Expression Is a Feature of Rare Adult Human Breast Epithelial Cells

AXL is expressed in rare epithelial cells in normal breast epithelium.

(A–D) (A) Multi-color immunofluorescence analysis of normal breast epithelium biopsies (n = 20). The ducts shown in (A–D) are formalin-fixed paraffin-embedded (FFPE) tissue sections stained with monoclonal antibodies against AXL (MAB10C9, white), MEP-specific cytokeratin 14 (K14, red), and luminal epithelial-specific cytokeratin 19 (K19, green); nuclear counterstain (DAPI, blue).

(E-H) Cryosections of normal human breast epithelium stained with monoclonal antibodies against: (E) AXL (ab21965, green), (F) K19 (magenta), (G) K14 (red). Overlay (H) reveals the areas of co-localized expression of AXL, K19, and K14 (white) in the lobular acini.

(I) Chromogenic IHC of AXL (ab21965, HRP-DAB brown) on FFPE sections of human mammary tissue. Counterstain by hematoxylin (blue).

(J–M) RNA *in situ* hybridization (RNA-ISH) on FFPE breast tissue specimens reveal the localization and distribution of (J) *AXL* mRNA transcripts, and (K) mRNA transcripts of the AXL-ligand *GAS6*. Each dot (brown, HRP-DAB) represents a single RNA molecule. (L and M) Histo-score analysis was performed to quantify the heterogeneity of the *AXL* and *GAS6* mRNA transcripts within the breast epithelium at the single cell level. The Histo-score of transcript expression was determined by categorizing epithelial cells in five predefined bins based on the number of transcripts per cell. Distribution (% of cells/bin) as well as Histo-scores provided on a range of 0-400 is given.

Figure 1. *Continued*

(N) Dual RNA ISH on paraffin-embedded section of normal human breast specimen reveal the spatial distribution and juxtaposition of *AXL* (AP-based Fast Red) and *GAS6* (HRP-based Green) mRNA transcripts within the normal human mammary epithelium. Counterstain by hematoxylin (blue).

The ducts shown in (A–D), (I), and (M–K), and the lobular acini shown in (E–H) are obtained from tumor biopsies from different patients.

same constellation of markers suggests that AXL may be a marker and regulator of multipotent cells in the human mammary epithelium.

KIT+/AXL + Primary HMECs Display a Unique Transcriptional Profile

We next examined the distribution of AXL expression relative to KIT *in situ*. Immunofluorescence staining of normal breast tissue revealed that KIT^+AXL^+ breast epithelial cells were predominantly positioned basally relative to KIT^+AXL^- staining cells that were positioned adjacent to the lumen (Figure 3A). Primary HMEC were enriched by FACS based on expression of KIT, and AXL was found to be expressed by 16% of the KIT^+ epithelial population, thus representing about 1% of the total primary mammary epithelial cell population (Figure 3B). To further delineate the difference between these epithelial populations, we sorted KIT^+AXL^+ and KIT^+AXL^- cells, and $CD227^+CD10^-$ LEP and $CD227^-CD10^+$ MEP subpopulations from primary HMEC at fourth passage (from two different women) and performed whole-genome expression analysis. Unsupervised hierarchical clustering identified distinct KIT^+AXL^+, KIT^+AXL^-, LEP, and MEP populations (Figure 3C). Principal component analysis of gene expression data revealed strong separation of KIT^+AXL^+, LEP and MEP populations, whereas the KIT^+AXL^- HMEC showed greater similarity to differentiated LEPs (Figure 3D). These results are consistent with the hypothesis that KIT^+AXL^+ cells represent a distinct breast epithelial progenitor population compared to the KIT^+AXL^- population.

AXL Kinase Activity Is Required for Self-Renewal and Acini Formation in Primary HMECs *Ex Vivo* Assays

To address the function of AXL signaling during differentiation, we cultured HMEC in the presence of an AXL-specific small molecule tyrosine kinase inhibitor (TKI) and monitored changes in the percentage of LEPs during subsequent passages. Standard *in vitro* culture of HMEC does not maintain the LEP population effectively, with an observed half-life of 3.8 $\pm$ 0.2 days due to the favored expansion of cells with basal properties, such as MEP (Figure 3E) (Garbe et al., 2012). Addition of a selective AXL TKI (bemcentinib, 600 nM) (Holland et al., 2010) counteracted LEP loss in culture (observed LEP half-life of 11.9 $\pm$ 5.9 days; $p = 0.43$), consistent with a pro-luminal differentiation effect, whereas a KIT TKI (imatinib, 1 μM) did not significantly alter LEP half-life (5.8 $\pm$ 0.5 days) (Figure 3E). Next, we assessed the requirement of AXL signal transduction for *in vitro* secondary mammosphere formation by HMEC enriched for KIT expression through two passages. Secondary mammosphere formation assays are frequently used a measure of self-maintenance activity. Secondary mammosphere formation was not affected by treatment with imatinib, but was reduced more than 4-fold by treatment with the AXL-inhibitor bemcentinib (Figure 3F). Formation of multi-lineage acini in 3D laminin-rich ECM (lrECM) was also significantly inhibited by treatment with bemcentinib, and only a few single K19-staining cells were observed in culture post-treatment (Figures 3G and 3H). Functional *ex vivo* assays showed that AXL kinase activity is required for self-renewal and maintenance of multi-lineage differentiation potential of AXL^+KIT^+ HMECs. Taken together, *in situ*, multiparameter cytometry, gene expression, and functional cell-based *ex vivo* analyses of primary human mammary epithelia align and suggest that AXL^+/KIT^+ cells exhibit multipotent activity. AXL^-/KIT^+ cells reside in the luminal compartment and exhibit activity consistent with luminal-biased progenitors. Our data do not establish a direct hierarchy between the two cell types.

AXL Is Required for Regeneration of Mouse Mammary Glands upon Transplantation

To explore the role of AXL in mouse mammary epithelia, we examined the mammary glands from a mouse strain that carries a targeted *LacZ* gene knock-in mutation that disrupts AXL protein expression (B6.129P2-$Axl^{tm1Dgen}$/J; Figures S2A and S2B). Analysis of the mammary glands of nulliparous adult expressing $Axl^{+/+}$ (wild type) mice and the functional knockout $Axl^{LacZ/LacZ}$ mice showed no statistically significant difference in estrogen receptor alpha (ESR1), progesterone receptor, or proliferation marker Ki67 (Figures 4A, S3B, and S3D). These results indicated that differentiated lineages present in the luminal compartment of $Axl^{LacZ/LacZ}$ glands were similar to wild type (Figures S3B and S3D). Morphometric analysis of H&E stained FFPE tissue sections revealed a significant increase in the average caliber (cross-sectional area) of ducts from

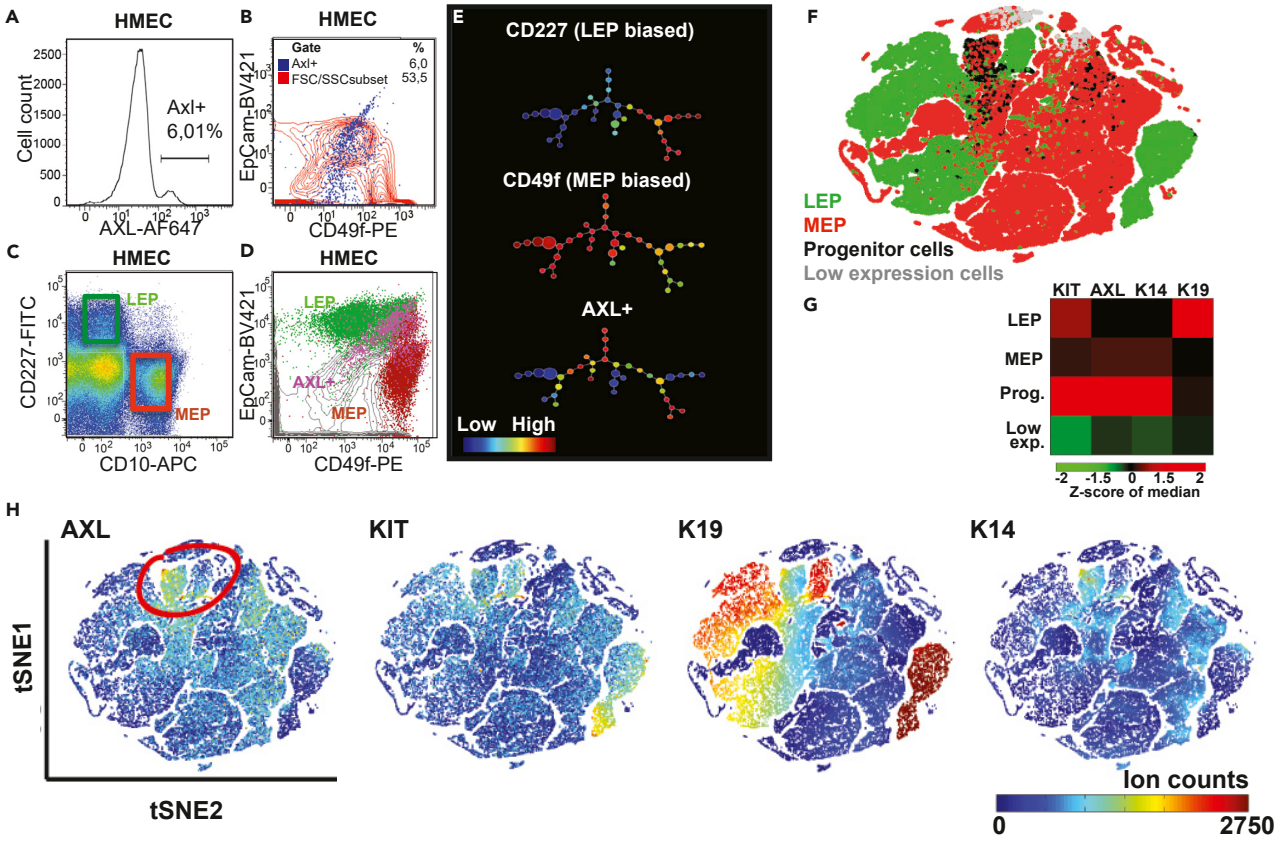

Figure 2. Phenotypic Characterization of AXL-Expressing Cells in Human Breast Epithelium

Analysis of AXL expression by flow cytometry of primary human breast epithelial cells (HMECs) isolated from patient reduction mammoplasty tissue samples.

(A) Total surface AXL staining of human breast epithelial cells isolated from epithelial-enriched preparations of reduction mammoplasty samples (range: 1–6%, n = 5 different patient biopsies; 500,000 events collected for each flow cytometry experiment displayed).

(B–E) (B) EPCAM/CD49f staining pattern of AXL-expressing cells (blue; gate shown in (E) within total human breast epithelial cell population (red topography map) (C) CD227/CD10 staining pattern and gating of LEP (green box) and MEP (red box) populations in epithelial-enriched preparations from reduction mammoplasty samples. (D) EPCAM/CD49f staining pattern and resolution of epithelial hierarchy cell types in enriched human breast epithelial and residual stromal cells isolated from reduction mammoplasty samples show enrichment of AXL-expressing cells in the stem/progenitor subpopulation (E) Analysis of HMEC EPCAM/CD49f/CD227/CD10/AXL flow cytometry data (from Figures 1C and 1D; 500,000 events; two different patients) using spanning-tree progression analysis of density-normalized events (SPADE), a computational approach to determine cell hierarchies from multiparametric data (Qiu et al., 2011). The SPADE-generated HMEC hierarchical tree comprises a continuum of distinct cell subpopulations depicted as circles with radii corresponding to cell number. The predicted HMEC hierarchy shows common origin at the apex with two radiations, MEP biased and LEP biased populations, respectively. Relative expression of a surface marker on cells within the hierarchy is shown on a blue (low expression) to red (high expression) scale. LEP-biased cells that express CD227, MEP-biased cells that express CD49f, and AXL-expressing cells are shown superimposed onto the HMEC hierarchy. Differentiated LEP and MEP cell populations occupy the left and right lineage radiations respectively, while AXL is expressed primarily in the putative bipotent epithelial stem/progenitor subpopulations found at the apex of the hierarchical tree.

(F) High-dimensional mass cytometry-based analysis of primary human mammary epithelia reveals a progenitor population expressing AXL, KIT K14 and K19. Non-linear dimensionality reduction, t-distributed stochastic neighbor embedding (tSNE) (Amir El et al., 2013) created a projection of 29 marker expression in 2D. Each point depicts a single cell of dissociated uncultured breast epithelia from women <30 years old (merged and subsampled at 50,000 cells, n = 7) (Pelissier Vatter et al., 2018). The raw data have been transformed with arcsinh with the cofactor of 5. Intra-lineage subpopulations were identified as distinct clusters of cells with shared phenotypes using PhenoGraph software (Levine et al., 2015). Unsupervised clustering identified four distinct phenotypes of LEP (LEP1–4), seven types of MEP (MEP1–7), a progenitor subpopulation and a low-expressing cell phenotype. The LEP and MEP clusters were merged and the tSNE projection of the PhenoGraph clusters is represented.

(G) Heatmaps of *Z* score of KIT, AXL, K14 and K19 expression in PhenoGraph clusters of uncultured breast epithelia from women <30 years old (merged, n = 7).

(H) tSNE projection (generated as described in detail for (F)), showing the relative expression of AXL, KIT, K19, and K14, respectively. The relative expression of these markers is shown on a violet-blue (low expression) to red (high expression) rainbow scale representing ion-counts from 0-27,500/cell.

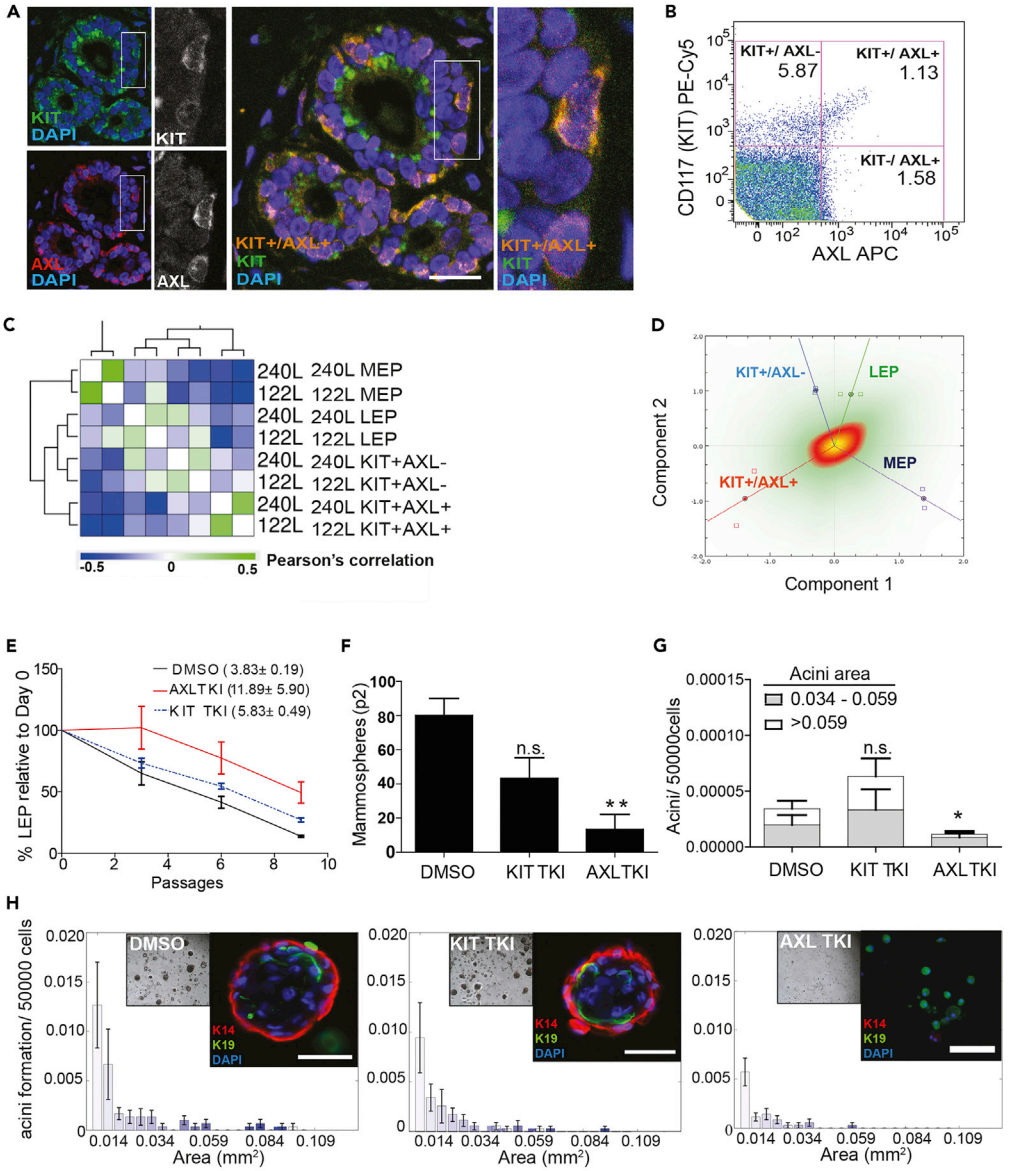

Figure 3. AXL Is Required for Self-Renewal and Generation of Differentiated Acini from Human Breast Epithelial Cells *Ex vivo*

(A) AXL is co-expressed with KIT on breast epithelial cells. Immunofluorescence of normal breast epithelial ducts in normal human breast biopsy FFPE sections (n = 6) show AXL (red), KIT (green), and AXL$^+$/KIT + double-positive cells (yellow). Nuclear counterstain by DAPI (blue). Scalebar: 30 μm.

(B) AXL expression defines a subpopulation of KIT-expressing breast epithelial progenitors. Flow cytometry-based quantification of KIT and AXL surface expression levels in human breast epithelial cells isolated from reduction mammoplasty samples (>100,000 sorted events; n = 3 patient samples). Quadrant gates and percentages of total events/gate are shown.

(C) AXL defines a distinct breast epithelial KIT-expressing progenitor subpopulation. Unsupervised hierarchical clustering based on whole-genome gene expression analysis (Illumina Bead Array) of FACS-isolated KIT$^+$/AXL$^+$, KIT$^+$/AXL$^-$, CD227$^+$ luminal (LEP) and CD10 + myoepithelial (MEP) subpopulations of HMEC cells (independent FACS analysis of HMEC strains 240L and 122L at passage 4). Weighted average linkage (WPGMA); Distance metric: Pearson's Correlation.

(D) KIT$^+$ progenitors lacking AXL show gene expression evidence of luminal commitment. Principal component correspondence plot derived from whole-genome gene expression analysis of KIT$^+$/AXL$^+$, KIT$^+$/AXL$^-$, CD227$^+$ luminal (LEP), and CD10$^+$ myoepithelial (MEP) FACS-isolated cells. X axis component variance: 22.387%; Y axis component variance: 17.091%; Total variance retained: 39.478%.

Figure 3. *Continued*

(E) Serial passage analysis of the percentage of $CD227^{+}/CD10^{-}$ luminal cells (LEP) in the HMEC strains 240L and 122L seeded at passage 4 in the presence of DMSO (control), KIT tyrosine kinase inhibitor (TKI) (imatinib, 1 μM) or AXL TKI (bemcentinib, 600 nM). %LEP was normalized to passage 0. Observed half-life values + - SD for each treatment condition (insert) were calculated using the formula: t * ln(2)/ln(N0/Nt) ($p < 0.05$).

(F) AXL activity is required for breast progenitor cell self-renewal as analyzed by secondary mammosphere formation generated by flow cytometry-enriched KIT + human mammary epithelial cell progenitors treated with DMSO (control), KIT TKI (imatinib, 1 μM), or AXL TKI (bemcentinib, 600 nM). Y axis represents total number of secondary mammospheres formed per well (mean ± S.E.M., n = 72; **p = 0.0075, t test).

(G) AXL is required for efficient formation of bilayered epithelial organoids in laminin-rich ECM assays. Image analysis of phase contrast images of mammary acini-like colonies formed from flow cytometry-enriched KIT + human mammary epithelial cell progenitor cells in 3D embedded laminin-rich ECM (lrECM) (matrigel), treated with DMSO (control), KIT TKI (imatinib, 1 μM), and AXL TKI (bemcentinib, 600 nM), respectively. Number of acini formed per 50.000 sorted KIT^{+} progenitor cells (mean ± S.E.M., n = 72; p values derived from t test) is shown by size distribution (Acini area: mm^2).

(H) Size distribution of organoids formed under the conditions described i (G) (Area: mm^2). Brightfield images and immunofluorescence analysis of representative organoids (inserts) display cytokeratin 14 (K14, red); cytokeratin 19 (K19, green); and nuclear counterstain: DAPI (blue). Scalebar 50 uM.

$Axl^{LacZ/LacZ}$ mice (n = 9) compared to ducts from wild type mice (n = 7, $p < 0.0001$) (Figure 4C). Image analysis of ductal diameters in carmine alum stained mammary gland whole mounts from 16-week-old $Axl^{LacZ/LacZ}$ (n = 9) and $Axl^{+/+}$ wild type mice (n = 8) confirmed differences in the overall size distributions (Figures 4B and S3A). β-galactosidase histochemistry revealed basal localization of *LacZ*-expressing cells in adult ducts (Figure 4D), sites where mouse mammary multipotent epithelial stem cells are thought to reside (Joshi et al., 2012). Mammary ducts from $Axl^{LacZ/LacZ}$ glands stained by immunofluorescence for detection of transgene product Beta-galactosidase in combination with MEP-marker K5 and LEP marker K8 confirmed the basal localization of the cells harboring the *LacZ* transgene (Figure 4E).

The observed phenotype of $Axl^{LacZ/LacZ}$ mammary glands is consistent with the viability of *Axl*-knockout animals; however, we speculated that forced postnatal regeneration of the mammary epithelia would exert sufficient stress to overcome compensatory mechanisms and reveal a more penetrant *Axl*-null phenotype. Thus, we evaluated the effect of AXL on mammary gland reconstitution upon transplantation of sorted cells in serial dilution. Lineage-negative (*i.e.* $CD45^{-}$, $CD31^{-}$, $CD11b^{-}$) AXL-expressing cells were enriched from dissociated $Axl^{+/LacZ}$ and $Axl^{LacZ/LacZ}$ adult mammary glands by FACS using the fluorogenic β-galactosidase substrate fluorescein Di-β-D-galactopyranoside (FDG). An FDG^{high} gate (highest 5%) was used to enrich for AXL-expressing cells, while AXL-negative cells were sorted using an FDG^{low} gate (lowest 65%) (Figure 4F). Serial dilutions of cells sorted on the basis of FDG (from 10,000 to 100 cells) were implanted into cleared fat pads of recipient prepubescent nude mice. Eight weeks post-transplantation, the mammary glands were harvested, fixated, and whole mount stained with carmine alum to visualize epithelial outgrowths. Mammary repopulating units (MRUs) frequencies were estimated by extreme limiting dilution analysis. FDG^{high} $Axl^{+/LacZ}$ cells readily repopulated the cleared fat pads with extensive mammary epithelial trees, whereas FDG^{low} $Axl^{+/LacZ}$ cells displayed a significantly reduced MRU frequency, as did the $Axl^{LacZ/LacZ}$ cells (Figures 4G and 4I). Hence, sorting for AXL expression enriched for adult murine mammary cells with repopulating activity in *ex vivo* organ reconstitution assay.

A number of previous reports show that luminal-biased progenitor cells cultured in 3D lrECM form hollow acini, whereas isolated MRU-competent MaSC form dense, pleomorphic structures (Lim et al., 2009; Shackleton et al., 2006; Stingl et al., 2006; Guo et al., 2012). FACS-isolated FDG^{high} mammary epithelial cells from $Axl^{+/LacZ}$ mice formed solid basal/stem-like colonies in lrECM characteristic of regenerative MaSC (Figures 4H and 4J upper row), whereas the FACS-isolated FDG^{high} mammary epithelial cells from $Axl^{LacZ/LacZ}$ mice formed significantly less colonies, and the colonies were predominantly well differentiated bilayered acini with basal K5 expressing and luminal K8 expressing compartments of cells (Figures 4H and 4J lower row).

Transcriptome of Sorted AXL + Mammary Cells Are Enriched in Genes Characteristic of Sorted MaSC Populations

Transcriptomes from FACS sorted FDG^{high} and FDG^{low} cells isolated from $Axl^{+/LacZ}$ adult mammary glands were then compared to previously published gene expression signatures from sorted mammary epithelial populations (Lim et al., 2009). Consistent with the functional analyses described above, the sorted FDG^{high} cell population isolated from $Axl^{+/LacZ}$ mammary glands displayed significant transcriptional similarity with

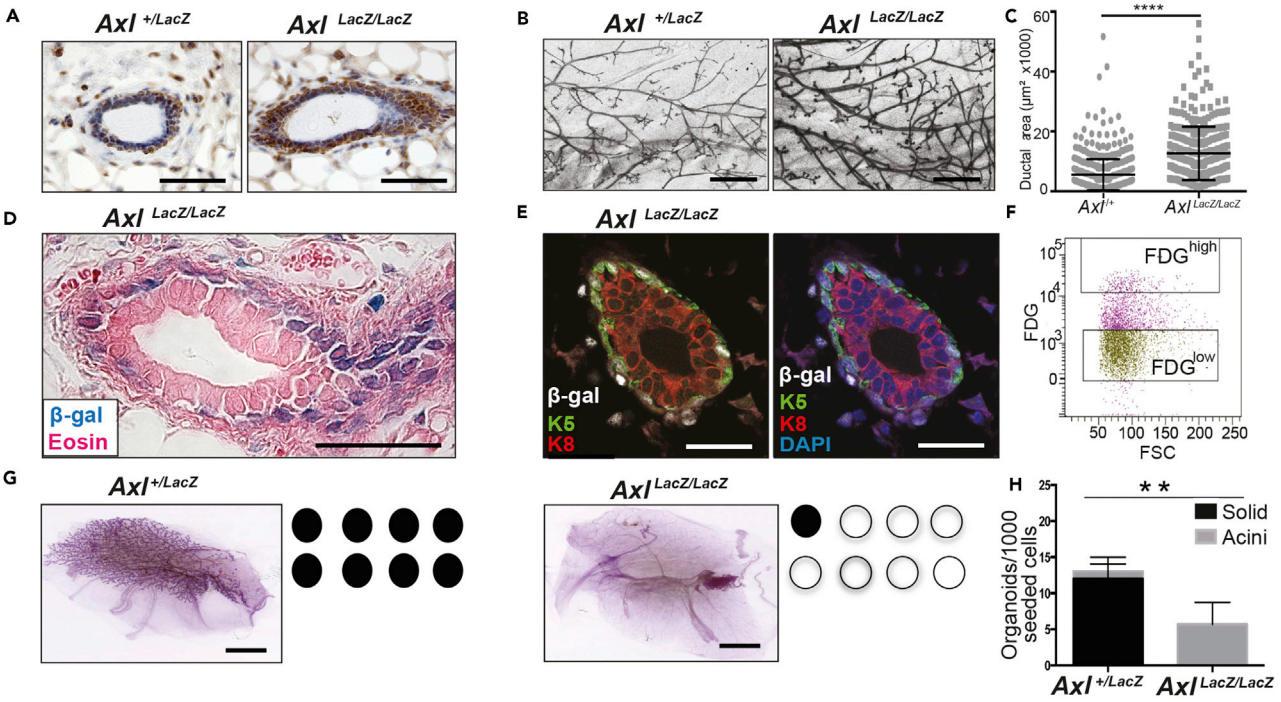

I

Genotype	Mammary cell subpopulation	No. cells injected	No. positive outgrowths	Repopulating frequency (95% CI)
Axl$^{+/LacZ}$	FDG^{high}	1000 100	8/8 8/8	1 (1/86 – 1)
	FDG^{low}	10000 1000 100	4/7 3/8 0/8	1/7569 *** (1/17406 - 1/3292)
Axl$^{LacZ/LacZ}$	FDG^{high}	10000 1000 100	8/8 2/8 1/8	1/2245 *** (1/5373 - 1/938)
	FDG^{low}	10000 1000 100	6/8 1/8 0/8	1/7388 *** (1/16209 - 1/3368)

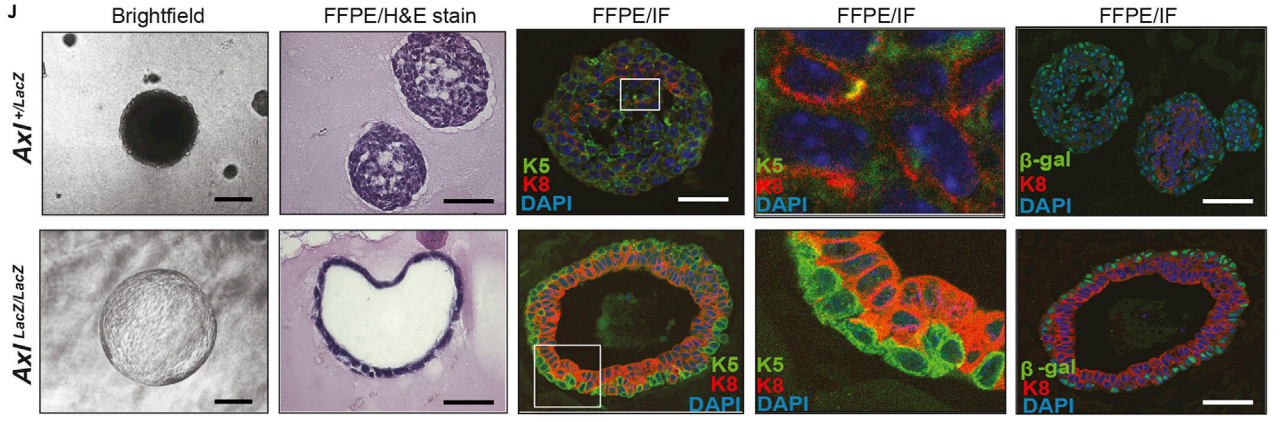

Figure 4. AXL Is Required for Regeneration of Mouse Mammary Glands upon Transplantation

(A) Immunostaining of FFPE sections of mammary glands from adult heterozygous *Axl*$^{+/LacZ}$ mice and homozygous functional AXL knockout *Axl*$^{LacZ/LacZ}$ of the B6.129P2-*Axltm1Dgen/J* mice revealed no significant difference in estrogen alpha receptor (ESR1) expression. Quantification is shown in Figure S3A. Scalebar: 100 μm.

(B) Carmine alum stained whole mounts of mammary glands from adult *Axl*$^{+/LacZ}$ and *Axl*$^{LacZ/LacZ}$ mice. Quantification of ductal diameter based on whole mounts are shown in Figure S3A. Scalebar: 250 μm.

(C) Morphometric histological analysis of HE stained mammary epithelial ducts from 16-week-old *AXL*$^{+/+}$ (n = 7) and *Axl*$^{LacZ/LacZ}$ (n = 9) mice. Quantification of the epithelial ducts were evaluated from HE stained FFPE sections. Both inguinal glands were harvested and included in the analysis, and area of epithelial structures from 10 separate fields/gland were included in the analysis (Mann-Whitney $p < 0.0001$).

(D) AXL promoter drives β-galactosidase expression in the two *AxlLacZ* alleles of homozygous *Axl*$^{LacZ/LacZ}$ mice. Whole mount beta-galactosidase histochemistry reveal the transgene expression from Axl promoter activity of mammary epithelial ducts. Glands were FFPE embedded post-staining and sections counterstained by eosin. Scalebar: 50 μm.

(E) Immunofluorescent staining of β–galactosidase (white), K8 (red), and K5 (green) reveal the localization of transgene expressing cells relative to the luminal (K8+) and basal (K5+) population in mammary epithelial ducts of homozygous *Axl*$^{LacZ/LacZ}$ mice. Image without DAPI (blue) nuclear stain is displayed the right to allow better visual inspection of the transgene expression (white) relative to K8 (red) and K5 (green). Scalebar: 30 μm.

(F and G) (F) FACS sorted cells expressing high (5% upper gate) and low (65% lower gate) cells were used for subsequent *in vitro* assays and limiting dilution transplantation assays (G) Representative whole mount image of cleared mammary fat pad repopulated by 100 FDG^{high} cells from heterozygous *Axl*$^{+/LacZ}$ mammary gland (left panel). Repopulating mammary epithelial outgrowths were found in 8/8 animals in this group (filled black circles). Representative whole mount image of mammary gland of animal reconstituted with 100 FDG^{+} cells from homozygous *Axl*$^{LacZ/LacZ}$ mammary glands (right panel). Repopulating mammary epithelial outgrowths were observed in 1/8 animals in this group (filled black, and empty circles, respectively). Data from one of three representative experiments are shown. Scalebar: 0.5 mm.

(H) Quantification of solid (black shaded bars) and acinar (gray shaded bars) *in vitro* colonies per 1000 seeded cells. Solid organoids were significantly reduced in the cultures derived from *Axl*$^{LacZ/LacZ}$ animals (t test: $p = 0.0023$).

(I) Limiting dilution *in vivo* mammary transplantation assay of FDG^{high} and FDG^{low} cell populations. The number of mammary outgrowths per transplantation group were quantified 8 weeks post-implantation, and the stem cell frequency and confidence intervals were calculated by limiting dilution analysis using Extreme Limiting Dilution Analysis (ELDA) software (http://bioinf.wehi.edu.au/software/elda/) (Hu and Smyth, 2009).

(J) Images of of mammary epithelial cells in 3D embedded organoids derived from *Axl*$^{-/LacZ}$ cells (upper row) and *Axl*$^{LacZ/LacZ}$ cells in 3D laminin-rich ECM (lrECM) culture (lower row) reveal the undifferentiated solid organoids derived from *Axl*$^{-/LacZ}$ and the differentiated acini formed by *Axl*$^{LacZ/LacZ}$ cells. As indicated, images represent (from left to right) brightfield images of live organoid cultures; HE stained organoids in formalin-fixed paraffin embedded (FFPE) sections, and immunofluorescence (IF) of FFPE sections with the markers K5 (green), K8 (red) and K5/K8 co-staining (yellow). The pictures to the right in the panel show beta-gal (green), K8 (red). Counterstain by DAPI (blue). Scalebars: 50 μm.

MaSC populations enriched using previously described markers (CD49f^{hi} CD29^{hi} CD24^{+} Sca1-subset) (Figures 5A and 5B). Indeed, CD61/CD49f flow cytometry analysis of dissociated mammary glands showed an increase in the luminal progenitor and LEP populations, and a slight reduction of the basal/stem population in cells from *Axl*$^{LacZ/LacZ}$ mice compared to *Axl*$^{+/LacZ}$ mice (Figure 5C). Whole mount adult mammary gland epithelia from *Axl*$^{LacZ/LacZ}$ mammary glands displayed a significant reduction in the number of alveolar buds at ductal termini compared to *Axl*$^{+/+}$ mammary glands (Figure 5D).

We hypothesized that AXL regulation of MaSC luminal potency in adult mammary gland regeneration could be governed by juxtacrine interactions between GAS6-producing LEP and AXL-expressing MaSC. Warfarin has previously been shown to be a well-tolerated inhibitor of GAS6-AXL signaling (Kirane et al., 2015). Thus, to test this model, we treated adult mice (12 weeks old) for 5 months with warfarin administered *ad libitum* in the drinking water to inhibit post-translational glutamic acid gamma-carboxylation of GAS6. Gamma-carboxylation of GAS6 has been shown to be required for strong AXL activation, and warfarin, a gamma-carboxylation inhibitor, converts GAS6 into a selective AXL antagonist (Lew et al., 2014; Kirane et al., 2015). Analysis of whole mounted adult mammary glands after 5 months of warfarin treatment demonstrated a significant reduction in the number of terminal alveolar buds in the warfarin treated group (Figure 5E), which phenocopied the *Axl*$^{LacZ/LacZ}$ animals (Figure 5D). A significant reduction in the number of terminal alveolar buds/gland was furthermore detected in pubescent warfarin treated mice (Figures S4A–S4C). Collectively, these results are consistent with a pro-differentiation phenotype of mammary glands of nulliparous adult *Axl*-null animals, as well as in AXL-antagonized wild type animals.

AXL MaSC Regulation Is Associated with Breast Cancer

We next examined whether gene signatures of normal AXL^{+} MaSC were an underlying feature of mammary tumors. Gene set enrichment analysis was used to detect the most differentially expressed genes between sorted FDG^{high} *Axl*$^{+/LacZ}$ and *Axl*$^{LacZ/LacZ}$ mammary cells. A signature comprising 33 downregulated and 37 upregulated genes was identified (rank product test, Table S1). Genes in this set have not been previously associated with MaSC, and thus may represent an unprecedented facet of the

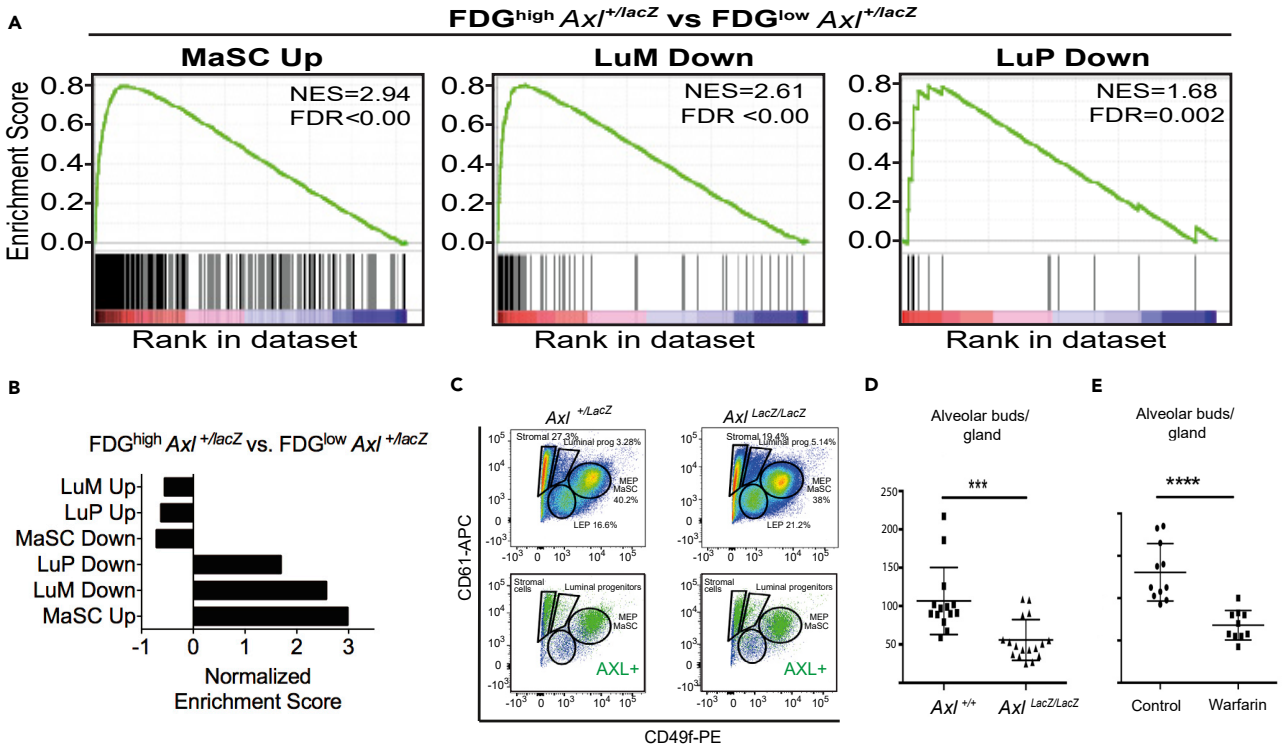

Figure 5. Gene Signatures Associated with Mammary Stem Cells (MaSC Population) Are Enriched in Murine Mammary Gland AXL + Cells and Loss of AXL Promotes Differentiation

(A) The gene set enrichment analysis of FDG^{high} versus FDG^{low} populations of *Axl*$^{-/LacZ}$ mammary cells revealed high similarity with published gene expression datasets from the MaSC-population enriched using standard markers (Lim et al., 2009). Enrichment plots for: MaSC = mammary stem cells; LuM = Luminal mature; LuP = Luminal progenitors, are shown. The top portion of the plot shows the running enrichment score for the gene set (green line) as the analysis moves along the ranked list of genes (x axis; red color indicates genes with higher expression and blue indicates low expression when the two gene-sets are compared). NES = normalized Enrichment Score. FDR = False discovery rate.

(B) The gene set enrichment analysis of FDG^{high} versus FDG^{low} populations of *Axl*$^{-/LacZ}$ mammary cells. NES = Normalized Enrichment Score is given for the comparison with the previously described gene signatures of MaSC = mammary stem cells; LuM = Luminal mature; LuP = Luminal progenitors (D) The gene set enrichment analysis of FDG^{high} versus FDG^{low} populations of *Axl*$^{LacZ/LacZ}$ mammary cells.

(C) Expression of CD61 and CD49f in lineage-negative cells isolated from *Axl*$^{-/LacZ}$ (left) and *Axl*$^{LacZ/LacZ}$ (right) mammary glands. Gating and percentage of total cells for different mammary cell populations is shown. Back gating of FDG^{high} cells confirm that AXL expression more prominent in the CD49f^{hi}/CD61^{+} MEP/MaSC population than in the CD49f^{low}/CD61^{low} LEP population.

(D) Quantification of alveolar buds at the termini of ducts of mammary glands were performed on whole mounts from *Axl*$^{+/+}$ (wild type, n = 8) and *Axl*$^{LacZ/LacZ}$ (AXL-null, n = 8) mice, 2 inguinal glands per animal (t test, $p < 0.0001$).

(E) Quantification of alveolar buds at the termini of ducts of mammary glands from mice treated for 5 months with warfarin (1 mg/L in drinking water). Quantification were performed on inguinal mammary gland whole mounts (n = 10 control glands, n = 10 warfarin treated glands), p=<0.0001, t test.

regenerative adult MaSC cell state (Figure 6A and Table S1). Notably, the AXL MaSC gene signature (AXL-stem) is not significantly enriched for core EMT genes. The generic EMT score captures the universal features of EMT based on expression of 315 EMT-related genes, and computed EMT scores range from −1 (epithelial) to 1 (mesenchymal) (Tan et al., 2014). The FDG high sorted cell population of *Axl*$^{+/LacZ}$ mice has a mean generic EMT score of 0.24, while FDG high sorted cells of *Axl*$^{LacZ/LacZ}$ mice have a mean generic EMT score of 0.21. Thus, these comparable intermediate mesenchymal EMT scores support a heretofore unappreciated role for AXL signaling in epithelial plasticity more generally, rather than maintaining EMT *per se*.

We and others have previously showed that AXL protein and mRNA expression is frequently detectable in basal-like breast cancer subtypes (Gjerdrum et al., 2010; Blick et al., 2010). The AXL-stem signature correlated with the degree of basal-like gene expression in the Metabric breast cancer patient cohort (Curtis et al., 2012) (Figure 6B) and was significantly elevated in basal-like breast tumor subtypes (PAM50 and IC10 subtypes; Figures 6C and S5). Furthermore, the AXL-stem score was

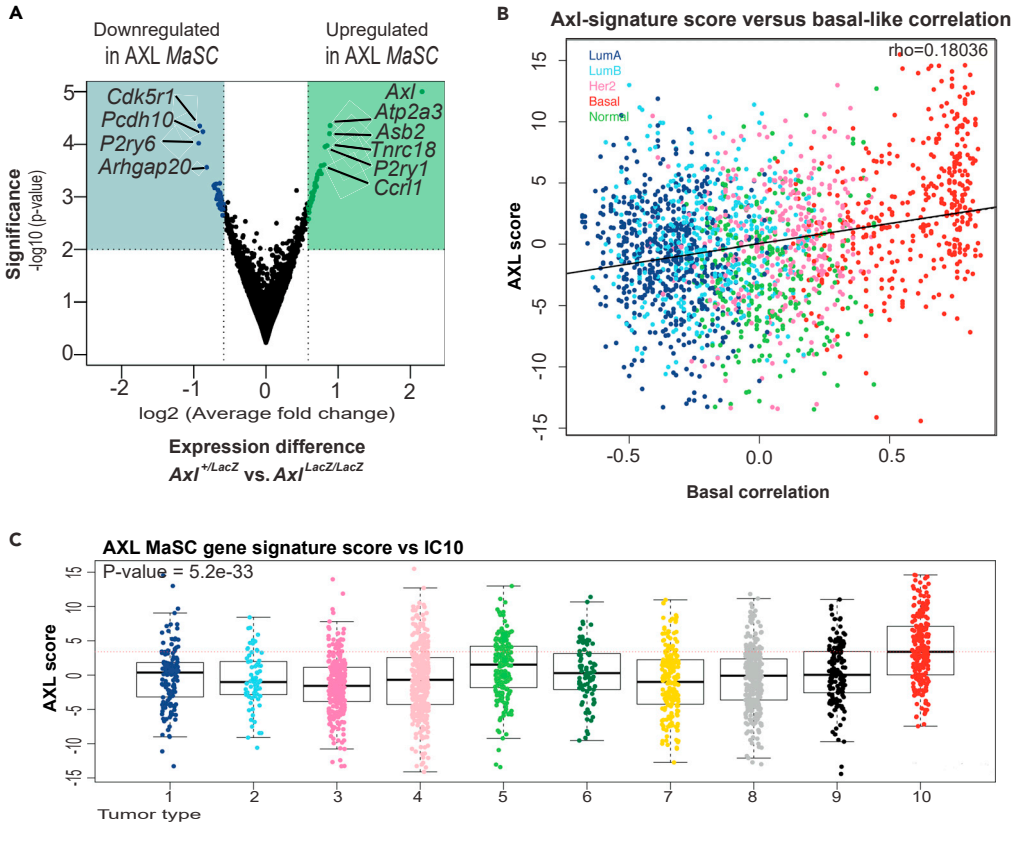

D

Univariate analysis*

	HR (95% CI)	*P*-value
AXL score	**1.0256** (1.008-1.044)	0.00496

Multivariate analysis*

	HR (95% CI)	*P*-value
Tumor grade	1.5254 (1.311-1.775)	4.52e-08
Lymph node status	1.8961 (1.692- 2.125)	2,00E-16
AXL score	**1.0242** (1.006-1.043)	0.00899

Figure 6. AXL MaSC Regulation Is Associated with Breast Cancer

(A) Volcano plot of significance versus fold gene expression change between the FDGhigh populations from $Axl^{+/LacZ}$ and $Axl^{LacZ/LacZ}$ adult mouse mammary epithelial cells. The most highly differentially expressed genes (cutoff: 1.5-fold change) are shaded.

(B) The Metabric breast cancer patient cohort (n = 1,980 patients) (Curtis et al., 2012) was interrogated with the AXL MaSC gene signature (AXL-stem, Table S1) to access the distribution correlated with the degree of basal-like gene expression in breast cancer ($\rho = 0.181$, $p = 5.5 \times 10\text{-}16$).

(C) The Metabric breast cancer patient cohort (n = 1,980) (Curtis et al., 2012) was interrogated with the AXL MaSC gene expression signature (AXL-stem, Table S1) to assess the influence of the AXL stem gene expression signature on clinical endpoints. AXL-stem score was significantly elevated in the core basal subtype of integrative cluster 10 (IC10) subtyped tumors from the Metabric breast cancer patient cohort (n = 1,980) (Curtis et al., 2012) ($p = 5.2 \times 10\text{-}33$, Kruskal-Wallis rank test).

(D) AXL-stem score was associated with breast cancer-specific outcome in a univariate model, stratified for hospital ($p = 0.00496$; hazard ratio: 1.026) and in a multivariate model correcting for grade and lymph node status ($p = 0.00899$; hazard ratio: 1.024, Cox proportional hazards regression, Breitling et al., 2004).

significantly associated with breast cancer-specific patient survival in a univariate model and in a multivariate model correcting for grade and lymph node status (Figure 6D). Hence, the AXL-dependent gene expression signature from murine MaSC correlates with clinical outcome in human breast cancer.

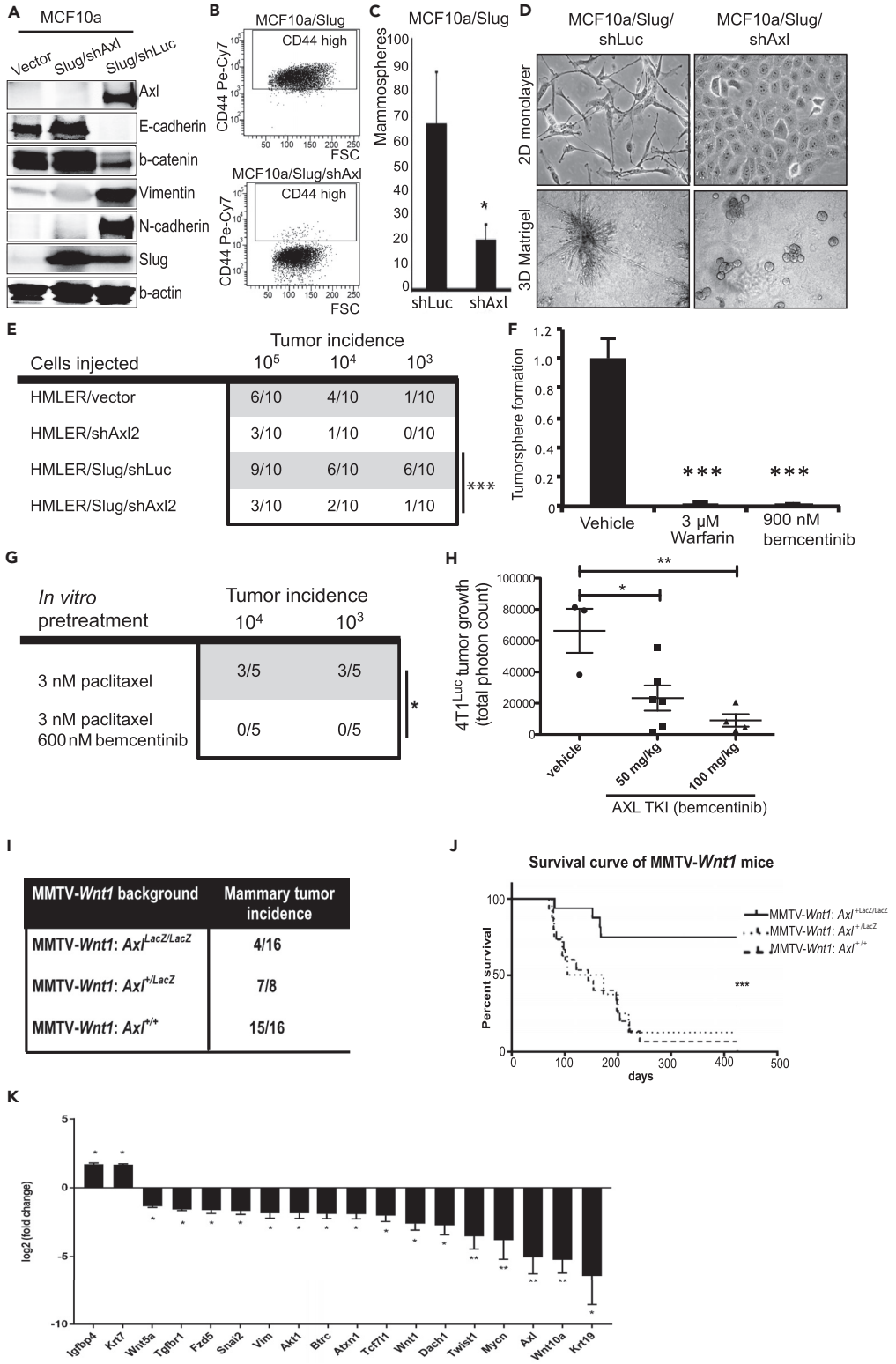

Figure 7. AXL Is Required for Breast Cancer Cell Phenotypic Plasticity, and Genetic Ablation of AXL Significantly Reduces Mammary Tumor Incidence in the MMTV-Wnt1 Mice

(A) AXL expression is required for SNAI2/Slug-induced EMT. MCF10a cells transduced with control or SNAI2/Slug retroviral expression vectors (GFP), and AXL-targeting shRNA (shAXL) or luciferase targeting control shRNA vectors

Figure 7. *Continued*

(shLuc) (RFP). Transduced cells were sorted based on GFP and RFP expression, and analyzed for AXL (140 kDa), SNAI2/Slug (30 kDa), and epithelial markers E-cadherin (135 kDa), β-catenin (92 kDa) and mesenchymal markers vimentin (55 kDa), and N-cadherin (100 kDa) by Western blotting. Loading control: β-actin (42 kDa).

(B) AXL-dependent loss of cell-surface glycoprotein CD44 shown by flow cytometric analysis of MCF10a/Slug/shAXL and MCF10a/Slug/shLuc cells.

(C) AXL expression is required for self-renewal activity. Quantification of mammosphere formation by MCF10a/Slug/shAXL and MCF10a/Slug/shLuc cells. Y axis represents total number of mammospheres formed per well (mean ± S.D., n = 5; *p < 0.05, t test).

(D) Phase contrast images of MCF10a/Slug/shAXL and MCF10a/Slug/shLuc cells grown as monolayer (2D, upper) and colony formation in 3D embedded laminin-rich ECM (lrECM) (matrigel, lower) reveal that Slug-mediated mesenchymal cell morphology and invasiveness are AXL-dependent.

(E) AXL is required for tumor initiation *in vivo*. Tumor incidence of HMLER/shLuc, HMLER/shAXL2 and HMLER/Slug/shAXL2 and HMLER/Slug/shLuc cells injected s.c. into recipient NOD-SCID mice at limiting dilutions (between 106-103 cells). HMLER/Slug/shAXL2 versus HMLER/Slug/shLuc, p = 0.0002, Fisher's exact test.

(F) Inhibition of AXL signaling using warfarin (3 uM) or AXL tyrosine kinase inhibitor (TKI) bemcentinib (900 nM) blocks 4T1 tumorsphere formation. Tumorsphere formation (day 7) was scored as Total Area (pixels2)/20,000 cells using ImageJ Analysis. Data plotted relative to vehicle (DMSO) treated cells (mean ± S.D., n = 6; ***p = 0.0005, t test).

(G) Reduced tumor incidence of 4T1 cells pretreated *in vitro* with 3 nM paclitaxel in the presence of 600 nM bemcentinib prior to injection injected into syngeneic host mice at limiting dilution versus *in vitro* treatment with 3 nM paclitaxel alone (p = 0.0108, Fisher's exact test).

(H) Inhibition of AXL kinase activity reduces mammary tumor formation. Bioluminescence (total photon counts) from tumors formed from orthotopically-implanted 4T1-luciferase (4T1Luc) cells at Day 7 treated with bemcentinib (50 and 100 mg/kg QD) (mean ± S.D., n = 6; *p < 0.05, **p < 0.005, one-way ANOVA).

(I) Spontaneous mammary tumor incidence in genetically modified animals carrying *MMTV-Wnt1* and the *AXLLacZ* knock-in allele. Comparison of tumor incidence between female AXL wild type *MMTV-Wnt1:Axl*$^{+/+}$ and AXL wild type *MMTV-Wnt1:Axl*$^{+/LacZ}$ and AXL-null *MMTV-Wnt1:Axl*$^{LacZ/LacZ}$ animals revealed that *Wnt1*-induced mammary tumor incidence (within 14 months) was significantly reduced in the AXL-null background (p = 0.0002, Fisher's exact test, two-tailed).

(J) Kaplan-Meier survival analysis of *MMTV-Wnt1* animals (Log rank (Mantel-Cox) test, Chi square: 14.98, p = 0.0001).

(K) Relative mRNA expression levels of a selection of significantly deregulated genes associated with EMT, CSC and WNT pathways in tumor cells isolated from *MMTV-Wnt1:Axl*$^{LacZ/LacZ}$ (n = 4) versus *MMTV-Wnt1:Axl*$^{+/+}$ (n = 6) animals. The expression levels of the *MMTV-Wnt1:Axl*$^{LacZ/LacZ}$ tumors were quantified relative to *MMTV-Wnt1:Axl*$^{+/+}$. Data are reported as mean fold changes ±SEM after normalization to the levels of housekeeping genes (ACTB, B2M, GAPDH, GUSB, HSP90AB1) in the panel. *p < 0.05, **p < 0.01 (Unpaired Student's t test).

AXL Signaling Is Required for Breast Cancer Cell Phenotypic Plasticity

Expression of the AXL-stem genes in breast cancer may reflect a co-option of MaSC-related regenerative activity that drives epithelial plasticity in breast cancer. SNAI2/Slug expression in immortalized human breast epithelial cell lines such as MCF10A engages an EMT-related stem cell program that results in expression of the AXL RTK (Gjerdrum et al., 2010; Vuoriluoto et al., 2011; Jokela et al., 2018). AXL knockdown were shown to reverse the SNAI2/Slug-dependent mesenchymal phenotype, restoring epithelial morphology and molecular marker expression, and blocking sphere-forming activity, without affecting SNAI2/Slug protein levels (Figures 7A–7D). Ectopic expression of AXL did not drive EMT in MCF10a (Figure S6). These results indicated that AXL signaling is required for SNAI2/Slug-dependent regulation of the EMT program. HMLER is a cell line generated by oncogenic transformation of HMECs that displays increased tumorgenicity upon overexpression of SNAI2/Slug (Mani et al., 2008). AXL knockdown significantly decreased tumor incidence independent of SNAI2/Slug overexpression in this model (Figure 7E). The 4T1 murine mammary tumor model enables tumor-forming experiments in isogenic, immune-competent mice. Tumorsphere formation with 4T1 cells was nearly abolished by treatment with warfarin (3uM) or with bemcentinib (900 nM) (Figure 7F). Pretreatment of 4TL with paclitaxel (3 nM) reduced tumor incidence following implantation, and pretreatment with paclitaxel and bemcentinib (600 nM) completely prevented tumor formation (Figure 7G). Furthermore, bemcentinib administered *in vivo* (both 50 and 100 mg/kg) decreased 4T1 tumor growth in syngeneic host mice (Figure 7H). These results support the notion that AXL is required to sustain epithelial plasticity traits that facilitate tumor formation in mammary glands.

AXL Is Required for Efficient *MMTV-Wnt1* Mammary Tumorigenesis

Mammary tumors arise in the *MMTV-Wnt1* model within an expanded MaSC pool and aberrant multipotent progenitor cells (Lim et al., 2009; Vaillant et al., 2008). Finally, in order to investigate the role of AXL in *Wnt1*-induced malignant transformation, we crossed the *AxlLacZ* knock-in and *MMTV-Wnt1* mouse strains. As expected, female *MMTV-Wnt1:Axl*$^{+/+}$ and *MMTV-Wnt1:Axl*$^{+/LacZ}$ animals developed mammary tumors with

high penetrance (Figure 7I). Strikingly, the incidence of mammary tumor development was reduced in the functional *Axl*-knockout *MMTV-Wnt1:Axl*$^{LacZ/LacZ}$ animals (Figure 7I), reflected also by the significantly increased survival of these animals (Figure 7J). Thus, AXL expression supported efficient *Wnt1*-mediated tumorigenesis, and comparison of gene expression in mammary tumor cells isolated from *MMTV-Wnt1* animals revealed significantly reduced expression of WNT, EMT, and cancer stem cell genes in rare tumors from the *Axl* $^{LacZ/LacZ}$ background (Figures 7K and S8).

DISCUSSION

AXL is expressed in multiple cancer types and is associated with poor clinical outcome and resistance to a number of therapies, including immune checkpoint inhibitors (Davidsen et al., 2017; Hugo et al., 2016; Goyette et al., 2018). While the presence of AXL in pathological contexts is increasingly well documented, our understanding of the role of AXL in normal physiology is lacking, with the current study providing evidence of a conserved role for AXL in human and murine mammary gland outside of innate immune regulation.

Supported by analysis of healthy human breast tissue, genetic mouse models, and patient tumor gene expression, our results are consistent with the interpretation that AXL is expressed by epithelial cells that are in a stem cell state. Our data suggest that AXL is so far a singular example of a putative MaSC marker that is conserved in human and mouse mammary epithelia. Data support the role of AXL as a regulator of a cellular plasticity program that endows a rare proportion of HMECs with the ability to transition between multipotent and differentiated states. Our multiparametric gene and marker expression data sets as well as functional *ex vivo* analyses are consistent with the interpretation that AXL is required for conditional expansion of a multipotent MaSC population in the adult mammary gland of both humans and rodents. In particular, AXL was found to regulate a unique gene set, AXL-stem, in regenerative MaSC that was inclusive of ARTN, is a GDNF-family/syndecan-3 ligand, a gene family associated with stem cell self-renewal (Merrell and Stanger, 2016), and linked to EMT and drug resistance traits in breast cancer (Kang et al., 2009; Ding et al., 2014). The AXL-stem signature identified in murine MaSC correlated with clinical outcome in the human Metabric breast cancer patient cohort. Significantly elevated in basal-like breast tumor subtypes (PAM50 and IC10 subtypes), the AXL-stem signature was correlated with poorer overall survival across all breast cancer subtypes. AXL may allow breast cancer cells the capacity to transition between distinct phenotypic states with different functional traits that support tumorigenesis (Visvader and Stingl, 2014). More work is necessary to determine if AXL signaling is a characteristic of long-lived multipotent MaSC or whether it is necessary for expansion and acquired multi-lineage differentiation potential during certain regenerative conditions (Rios et al., 2014; Van Keymeulen et al., 2011).

AXL was shown to be required for the efficient formation of bilayered acini in lrECM assays from FACS enriched KIT + HMECs, and AXL inhibition prevented LEP loss in 2D HMEC culture and significantly decreased self-renewal capacity in secondary mammosphere assays. Although we cannot rule out the possibility that AXL$^+$ MaSC are luminal-biased, both mammary transplantation in cleared murine fat pads and acinus formation assays with primary human cells showed a capacity for self-renewal and multi-lineage differentiation at least *ex vivo*. Multi-color immunofluorescence staining of mammary tissues showed that AXL + cells expressed also the intermediate filament proteins K14 and K19 that were located in a basal or suprabasal position, in ducts. FACS staining showed that AXL + cells were enriched among EpCAM$^+$/CD49f$^+$ cells. Our previous work showed that EpCAM$^+$/CD49f$^+$ HMECs that exhibited stem cell activity co-expressed K14 and K19 (Villadsen et al., 2007). EpCAM^{low}/CD10^{high} epithelial cells also were enriched for stem cell activities and were reported to express K14 and K18, but not K19 (Bachelard-Cascales et al., 2010). Taken together, we interpreted these findings such that cells in MaSC states have shared properties of MEP and luminal cells. From the human high-dimensional expression data, it is evident that the KIT^{+-} AXL$^-$ HMEC are more luminal lineage-biased, and their localization adjacent to the lumen, and the similarity of gene expression to CD227$^+$/CD10$^-$/KIT$^-$ luminal cells supported this interpretation. However, more work and lineage tracing experiments are needed to determine definitively the lineage potential of the AXL + mammary epithelial population.

A conundrum raised by our results is that Axl-null animals are able to develop functional mammary glands, yet upon *ex vivo* transplantation into cleared fat pads of recipient mice the sorted Axl-null epithelial cells showed a significant reduction in the ability to reconstitute the mammary tree. Relatedly, the GAS6-null mouse also develops functional mammary glands (Mills et al., 2018). Knockout of the TAM family member Mer did show a developmental phenotype during post-lactational involution as it was shown necessary for

mediating epithelial efferocytosis of apoptotic cells, but AXL and Tyro3 were explicitly not required for that process (Sandahl et al., 2010). The importance of the mammary gland for mammals implies strong evolutionary pressure to favor gland development with much redundancy. Indeed, we are not aware of any reports of gene knockouts that reach adulthood and have no mammary gland. AXL is an imprinted gene, which rather suggests that fine-tuned temporal and spatial regulation of AXL expression during embryonic development is crucial. AXL + epithelial cells were enriched for their ability to form mammary glands in the cleared fat pad assay, which may be a better representation of regeneration or even wound repair. Historically, a number of gene knockout animals have shown no overt phenotype until stressors were applied, and this may be an example in which AXL was essential for allowing the mammary epithelial cells to survive in, or even to establish, the regenerative niche. Furthermore, as we have noted above, the role of AXL in cancer progression is being increasingly appreciated and the regenerative or wound healing microenvironment has also been used to characterize the tumor microenvironment. Even though cell transfer and tissue regeneration assays are considered a gold standard for stem cell biology, it is worth recognizing that the assays are prone to disrupting solid tissues in a way that might be orthogonal to development.

A reasonable interpretation of our data is that AXL allows access to gene expression programs that repress the luminal phenotype. Hence, removal of signaling through the AXL pathway is sufficient to allow cells to access the luminal differentiation program. Indeed lineage-priming occurs in the expanded stem cell population during pregnancy prior to commitment along the alveolar lineage (Pal et al., 2013). Interfering with AXL expression in double-positive epithelial cells may push the progenitor profile into a different compartment, or the cells lose self-renewal abilities in favor of terminal differentiation due to a transition from a symmetric to an asymmetric mode of stem cell division. Although the mode of stem cell division was not directly addressed in this study, the increased mammary tumor incidence in the MMTV-Wnt model as well as the impact of AXL inhibition in *ex vivo* assays could support a model where AXL act as a mediator of symmetric self-renewing stem cell division, and the differentiation induced upon AXL inhibition is due to a switch to an asymmetric or symmetric differentiating stem cell division which is less advantageous for stem cell expansion and neoplastic transformation.

The striking reduction of Wnt1-driven mammary tumors in the Axl-null background was associated with a reduced expression of WNT-signaling genes (e.g. Wnt5a, Wnt10a, Wnt1, Fzd5, Mycn), genes associated with EMT (e.g. Twist1, Snai2, Vim), and K19 and Tgfb1/Tgfbr1 expression. It is tempting to speculate that AXL may support Wnt1-induced multipotent stem-like properties (Vaillant et al., 2008). Further characterization of the MMTV-Wnt1 tumor data is required; more mechanistic insights should be gathered to determine if Axl depletion leads to an impairment of Wnt signaling, or whether the effect is independent of Wnt.

We recently found that warfarin-use is associated with lower cancer risk in a large retrospective epidemiology study (Haaland et al., 2017). The vitamin K antagonist warfarin selectively inhibits gamma-carboxylation of Gla domain proteins, of which there are only 14 encoded in the human genome, most representing coagulation factors predominantly expressed in the liver. GAS6 is an outlier in this group with expression in several tissues and whose only known function is as the sole ligand for AXL (and a shared lower affinity ligand for MERTK/TYRO3). Of note, GAS6 is an estrogen inducible gene in mammary epithelial cells, and by bridging the kinase ectodomain and externalized phosphatidylserine (PS) displayed e.g on apoptotic cells, gamma-carboxylation of the GAS6 Gla domain is required for strong AXL activation, but not for MERTK/TYRO3 activation (Lew et al., 2014). Thus, "Gla-less" GAS6 is a specific AXL antagonist (Lew et al., 2014). Relevant to our warfarin experiments, and unaccounted for so far, is the possibility that other Gla domain proteins (periostin and osteocalcin) that are mainly expressed in the stroma were affected in a way that alters mammary epithelial activity.

Based on the data presented here we propose a working model where juxtracrine GAS6 and AXL interactions support microenvironmental PS-sensing and adult mammary gland stem cell expansion in the context of tissue damage and regeneration that deserves to be further explored in relevant models. Collectively, the results support further exploring aberrant AXL signaling as a therapeutic target in the treatment as well as chemoprevention of breast cancers.

Limitations of the Study

The study of human breast epithelial stem cells is hampered by a lack of experimental models and thus our current understanding of mammary gland biology is derived largely from rodent models. Although a

number of flow cytometric markers are used to enrich for MaSC, a consensus set of markers that identifies multipotent MaSC in both human and mouse mammary remain elusive. This lack of common markers and mechanistic understanding governing human and mouse multipotent MaSC has brought into question how congruent MaSC biology is between these two species, casting doubt on the relevance of results determined in mouse studies, particularly for breast cancer. Furthermore, it remains to be elucidated whether regeneration of adult mammary tissue from endogenous stem cells exploits the same molecular pathways used to establish the mammary epithelium during development. As the ability of sorted cells to form mammary glands in the cleared fat pad assay may be a better representation of regeneration, and the role of GAS6-AXL signaling in murine mammary gland development have not been addressed. From emerging high-dimensional data, one can speculate that a continuum of cells along the differentiation axis is far more complex than previously anticipated and remains to be explored further.

Resource Availability

Lead Contact

Further information and requests for resources and reagents should be directed to and will be fulfilled by the Lead Contact, James Lorens (jim.lorens@uib.no).

Materials Availability

All unique/stable reagents generated in this study are available from the Lead Contact upon request pending completed Materials Transfer Agreement.

Data and Code Availability

The CyTOF data reported in this paper is accessible through Mendeley: https://doi.org/10.17632/j7mrbgt3hh.1. The BeadChip array data of sorted cells from B6.129P2-Axltm1Dgen/J mice are accessible through GEO database, accession number: GSE156662: https://www.ncbi.nlm.nih.gov/geo/query/acc.cgi?acc=GSE156662.

METHODS

All methods can be found in the accompanying Transparent Methods supplemental file.

SUPPLEMENTAL INFORMATION

Supplemental Information can be found online at https://doi.org/10.1016/j.isci.2020.101649.

ACKNOWLEDGMENTS

The authors are grateful to Dr. Janice Nigro for invaluable advice, language and manuscript editing. Thanks to Sissel Vik Berge, Endre Stigen, Ingrid Gavlen, Bendik Nordanger, and Jason Toombs for excellent technical support, Brith Bergum and Marianne Enger at the Flow Cytometry Core Facility at UiB, and Endy Spriet and Hege Avsnes Dale at the Molecular Imaging Center, UiB. The authors thank Dr. Kjell Petersen, Computational Biology Unit and, Norwegian Bioinformatics Platform, UiB, for microarray analysis support. The authors are grateful to the staff at the animal facility at the University of Bergen for their skillful maintenance and care of the research animals. And finally, the authors express their thanks to the women that consented to the use of their reduction mammoplasty tissue and biopsy tissue for this research.

This work was partly supported by the Research Council of Norway through its Centers of Excellence funding scheme, project number 223250 (CCBIO affiliates). JBL was supported by grants from the Norwegian Research Council (grant number 204868), and Norwegian Cancer Society (grant number 190330). ML from the National Institutes of Health (R01AG040081 and R00AG033176), and United States Congressionally Directed Medical Research Program's Era of Hope Scholar Award (BC141351). ASTE was supported by an FRIPRO Mobility Grant Fellowship from the Research Council of Norway co-funded by the EU's seventh Framework Program's Marie Skłodowska Curie Actions (MSCA COFUND, grant agreement number 608695). Support by Legat for Forskning av Kreftsykdommer fund at UIB, and Familien Blix fund to ASTE for the conduct of this study is greatly appreciated. Graphical abstract was created with BioRender.com.

AUTHOR CONTRIBUTIONS

Conception and design: M.A.L, J.B.L. Development of methodology: A.S.T.E, K.W-L, S.B, F.A.P.V, R.V, C.T, M.M, S.G., M.R.S, M.A.L, J.B.L. Acquisition of data: (provided animals, acquired and managed patients, provided facilities, etc.): A.S.T.E, K.W-L, S.B, F.A.P.V, C.T, M.M, O.S. Analysis and interpretation of data (e.g., statistical analysis, biostatistics, computational analysis): A.S.T.E, K. W-L, S.B, F.A.P.V, M.L.L, R.V, S.D, S.D'M.P, C.T, M. M, P. P, N.M. S.M.A, S.N, M.R.S, R.V, T. S, R.A.B, O.S, N.H, T.Z.T, J.P.T, L.A.A, O.P, M.A.L, J.B.L. Writing, review, and/or revision of the manuscript: A.S.T.E, K.W-L, M.L.L, J.P.T, O.P, R.V, M.A.L, J.B.L. Administrative, technical, or material support (i.e., reporting or organizing data, constructing databases): R.V, S.N, L.H, G.G, M.R.S, T.S, R.A.B, O.S, N.H, L.A.A, O.P, M.A.L, J.B.L. Study supervision: M.A.L, J.B.L.

DECLARATION OF INTERESTS

J.B.L. is founder and shareholder of BerGenBio ASA. K.W.L., G.G. and J.B.L. are former or current employees of BerGenBio ASA. J.P.T. is scientific founder and CSO of Biocheetah Pte Ltd Singapore and consultant/shareholder Biosyngen Pte Lte Limited and ACTgenomics Taipei Taiwan. S.C. and R.A.B. signed Sponsored Research Agreements with BerGenBio ASA related to a separate research project. The remaining authors declare no conflict of interest.

Received: August 22, 2018
Revised: August 3, 2020
Accepted: October 2, 2020
Published: November 20, 2020

REFERENCES

Amir El, A.D., Davis, K.L., Tadmor, M.D., Simonds, E.F., Levine, J.H., Bendall, S.C., Shenfeld, D.K., Krishnaswamy, S., Nolan, G.P., and Pe'er, D. (2013). viSNE enables visualization of high dimensional single-cell data and reveals phenotypic heterogeneity of leukemia. Nat. Biotechnol. *31*, 545–552.

Antony, J., Tan, T.Z., Kelly, Z., Low, J., Choolani, M., Recchi, C., Gabra, H., Thiery, J.P., and Huang, R.Y. (2016). The GAS6-AXL signaling network is a mesenchymal (Mes) molecular subtype-specific therapeutic target for ovarian cancer. Sci. Signal *9*, ra97.

Bachelard-Cascales, E., Chapellier, M., Delay, E., Pochon, G., Voeltzel, T., Puisieux, A., Caron De Fromentel, C., and Maguer-Satta, V. (2010). The CD10 enzyme is a key player to identify and regulate human mammary stem cells. Stem Cells *28*, 1081–1088.

Billaud, M., and Santoro, M. (2011). Is co-option a prevailing mechanism during cancer progression? Cancer Res. *71*, 6572–6575.

Blanpain, C., and Fuchs, E. (2014). Stem cell plasticity. Plasticity of epithelial stem cells in tissue regeneration. Science *344*, 1242281.

Blick, T., Hugo, H., Widodo, E., Waltham, M., Pinto, C., Mani, S.A., Weinberg, R.A., Neve, R.M., Lenburg, M.E., and Thompson, E.W. (2010). Epithelial mesenchymal transition traits in human breast cancer cell lines parallel the CD44(hi/) CD24 (lo/-) stem cell phenotype in human breast cancer. J. Mammary Gland Biol. Neoplasia *15*, 235–252.

Breitling, R., Armengaud, P., and AmtmannHerzyk, A.P. (2004). Rank products: a simple, yet powerful, new method to detect differentially regulated genes in replicated microarray experiments. FEBS Lett *573*, 83–92.

Chen, L., Jenjaroenpun, P., Pillai, A.M., Ivshina, A.V., Ow, G.S., Efthimios, M., Zhiqun, T., Tan, T.Z., Lee, S.C., Rogers, K., et al. (2017). Transposon insertional mutagenesis in mice identifies human breast cancer susceptibility genes and signatures for stratification. Proc. Natl. Acad. Sci. U S A *114*, E2215–E2224.

Curtis, C., Shah, S.P., Chin, S.F., Turashvili, G., Rueda, O.M., Dunning, M.J., Speed, D., Lynch, A.G., Samarajiwa, S., Yuan, Y., et al. (2012). The genomic and transcriptomic architecture of 2,000 breast tumours reveals novel subgroups. Nature *486*, 346–352.

Davidsen, K.T., Haaland, G.S., Lie, M.K., Lorens, J.B., and Engelsen, A.S.T. (2017). The role of Axl receptor tyrosine kinase in tumor cell plasticity and therapy resistance. In *Biomarkers of the Tumor Microenvironment: Basic Studies and Practical Applications*. Switzwerland, L.A. Akslen and R.S. Watnick, eds. (Springer Press), pp. 351–376.

Ding, K., Banerjee, A., Tan, S., Zhao, J., Zhuang, Q., Li, R., Qian, P., Liu, S., Wu, Z.S., Lobie, P.E., and Zhu, T. (2014). Artemin, a member of the glial cell line-derived neurotrophic factor family of ligands, is HER2-regulated and mediates acquired trastuzumab resistance by promoting cancer stem cell-like behavior in mammary carcinoma cells. J. Biol. Chem. *289*, 16057–16071.

Dravis, C., Spike, B.T., Harrell, J.C., Johns, C., Trejo, C.L., Southard-Smith, E.M., Perou, C.M., and Wahl, G.M. (2015). Sox10 regulates stem/progenitor and mesenchymal cell states in mammary epithelial cells. Cell Rep. *12*, 2035–2048.

Eirew, P., Stingl, J., Raouf, A., Turashvili, G., Aparicio, S., Emerman, J.T., and Eaves, C.J. (2008). A method for quantifying normal human mammary epithelial stem cells with in vivo regenerative ability. Nat. Med. *14*, 1384–1389.

Fridriksdottir, A.J., Villadsen, R., Morsing, M., Klitgaard, M.C., Kim, J., Petersen, O.W., and Ronnov-Jessen, L. (2017). Proof of region-specific multipotent progenitors in human breast epithelia. Proc. Natl. Acad. Sci. U S A *114*, E10102–E10111.

Garbe, J.C., Pepin, F., Pelissier, F.A., Sputova, K., Fridriksdottir, A.J., Guo, D.E., Villadsen, R., Park, M., Petersen, O.W., Borowsky, A.D., et al. (2012). Accumulation of multipotent progenitors with a basal differentiation bias during aging of human mammary epithelia. Cancer Res. *72*, 3687–3701.

Giraddi, R.R., Chung, C.Y., Heinz, R.E., Balcioglu, O., Novotny, M., Trejo, C.L., Dravis, C., Hagos, B.M., Mehrabad, E.M., Rodewald, L.W., et al. (2018). single-cell transcriptomes distinguish stem cell state changes and lineage specification programs in early mammary gland development. Cell Rep. *24*, 1653–1666 e7.

Gjerdrum, C., Tiron, C., Hoiby, T., Stefansson, I., Haugen, H., Sandal, T., Collett, K., Li, S., Mccormack, E., Gjertsen, B.T., et al. (2010). Axl is an essential epithelial-to-mesenchymal transition-induced regulator of breast cancer metastasis and patient survival. Proc. Natl. Acad. Sci. U S A *107*, 1124–1129.

Goyette, M.A., Duhamel, S., Aubert, L., Pelletier, A., Savage, P., Thibault, M.P., Johnson, R.M., Carmeliet, P., Basik, M., Gaboury, L., et al. (2018). The receptor tyrosine kinase AXL is required at multiple steps of the metastatic cascade during HER2-positive breast cancer progression. Cell Rep. *23*, 1476–1490.

Guo, W., Keckesova, Z., Donaher, J.L., Shibue, T., Tischler, V., Reinhardt, F., Itzkovitz, S., Noske, A., Zurrer-Hardi, U., Bell, G., et al. (2012). Slug and Sox9 cooperatively determine the mammary stem cell state. Cell *148*, 1015–1028.

Haaland, G.S., Falk, R.S., Straume, O., and Lorens, J.B. (2017). Association of warfarin use with lower overall cancer incidence among patients older than 50 years. JAMA Intern. Med. *177*, 1774–1780.

Holland, S.J., Pan, A., Franci, C., Hu, Y., Chang, B., Li, W., Duan, M., Torneros, A., Yu, J., Heckrodt, T.J., et al. (2010). R428, a selective small molecule inhibitor of Axl kinase, blocks tumor spread and prolongs survival in models of metastatic breast cancer. Cancer Res. *70*, 1544–1554.

Hu, Y., and Smyth, G.K. (2009). ELDA: extreme limiting dilution analysis for comparing depleted and enriched populations in stem cell and other assays. J Immunol Methods *347*, 70–78.

Hugo, W., Zaretsky, J.M., Sun, L., Song, C., Moreno, B.H., Hu-Lieskovan, S., Berent-Maoz, B., Pang, J., Chmielowski, B., Cherry, G., et al. (2016). Genomic and transcriptomic features of response to anti-pd-1 therapy in metastatic melanoma. Cell *165*, 35–44.

Huo, Y., and Macara, I.G. (2014). The Par3-like polarity protein Par3L is essential for mammary stem cell maintenance. Nat. Cell Biol. *16*, 529–537.

Jokela, T.A., Engelsen, A.S.T., Rybicka, A., Pelissier Vatter, F.A., Garbe, J.C., Miyano, M., Tiron, C., Ferariu, D., Akslen, L.A., Stampfer, M.R., et al. (2018). Microenvironment-induced non-sporadic expression of the AXL and cKIT receptors are related to epithelial plasticity and drug resistance. Front. Cell Dev. Biol. *6*, 41.

Joshi, P.A., Di Grappa, M.A., and Khokha, R. (2012). Active allies: hormones, stem cells and the niche in adult mammopoiesis. Trends Endocrinol. Metab. *23*, 299–309.

Kang, J., Perry, J.K., Pandey, V., Fielder, G.C., Mei, B., Qian, P.X., Wu, Z.S., Zhu, T., Liu, D.X., and Lobie, P.E. (2009). Artemin is oncogenic for human mammary carcinoma cells. Oncogene *28*, 2034–2045.

Kirane, A., Ludwig, K.F., Sorrelle, N., Haaland, G., Sandal, T., Ranaweera, R., Toombs, J.E., Wang, M., Dineen, S.P., Micklem, D., et al. (2015). Warfarin blocks Gas6-mediated Axl activation required for pancreatic cancer epithelial plasticity and metastasis. Cancer Res. *75*, 3699–3705.

Lawson, D.A., Bhakta, N.R., Kessenbrock, K., Prummel, K.D., Yu, Y., Takai, K., Zhou, A., Eyob, H., Balakrishnan, S., Wang, C.Y., et al. (2015). Single-cell analysis reveals a stem-cell program in human metastatic breast cancer cells. Nature *526*, 131–135.

Levine, J.H., Simonds, E.F., Bendall, S.C., Davis, K.L., Amir, E.D., Tadmor, M.D., Litvin, O., Fienberg, H.G., Jager, A., and Zunder, E.R. (2015). Data-driven phenotypic dissection of AML reveals progenitor-like cells that correlate with prognosis. Cell *162*, 184–197.

Lew, E.D., Oh, J., Burrola, P.G., Lax, I., Zagorska, A., Traves, P.G., Schlessinger, J., and Lemke, G. (2014). Differential TAM receptor-ligand-phospholipid interactions delimit differential TAM bioactivities. Elife *3*, e03385.

Lilja, A.M., Rodilla, V., Huyghe, M., Hannezo, E., Landragin, C., Renaud, O., Leroy, O., Rulands, S., Simons, B.D., and Fre, S. (2018). Clonal analysis of Notch1-expressing cells reveals the existence of unipotent stem cells that retain long-term plasticity in the embryonic mammary gland. Nat. Cell Biol. *20*, 677–687.

Lim, E., Vaillant, F., Wu, D., Forrest, N.C., Pal, B., Hart, A.H., Asselin-Labat, M.L., Gyorki, D.E., Ward, T., Partanen, A., et al. (2009). Aberrant luminal progenitors as the candidate target population for basal tumor development in BRCA1 mutation carriers. Nat. Med. *15*, 907–913.

Lotsberg, M.L., Wnuk-Lipinska, K., Terry, S., Tan, T.Z., Lu, N., Trachsel-Moncho, L., Rosland, G.V., Siraji, M.I., Hellesoy, M., Rayford, A., et al. (2020). AXL targeting abrogates autophagic flux and induces immunogenic cell death in drug-resistant cancer cells. J. Thorac. Oncol. *15*, 973–999.

Lu, Q., and Lemke, G. (2001). Homeostatic regulation of the immune system by receptor tyrosine kinases of the Tyro 3 family. Science *293*, 306–311.

Ludwig, K.F., Du, W., Sorrelle, N.B., Wnuk-Lipinska, K., Topalovski, M., Toombs, J.E., Cruz, V.H., Yabuuchi, S., Rajeshkumar, N.V., Maitra, A., et al. (2018). Small-molecule inhibition of Axl targets tumor immune suppression and enhances chemotherapy in pancreatic cancer. Cancer Res. *78*, 246–255.

Mani, S.A., Guo, W., Liao, M.J., Eaton, E.N., Ayyanan, A., Zhou, A.Y., Brooks, M., Reinhard, F., Zhang, C.C., Shipitsin, M., et al. (2008). The epithelial-mesenchymal transition generates cells with properties of stem cells. Cell *133*, 704–715.

Merrell, A.J., and Stanger, B.Z. (2016). Adult cell plasticity in vivo: de-differentiation and transdifferentiation are back in style. Nat. Rev. Mol. Cell Biol. *17*, 413–425.

Meyer, A.S., Miller, M.A., Gertler, F.B., and Lauffenburger, D.A. (2013). The receptor AXL diversifies EGFR signaling and limits the response to EGFR-targeted inhibitors in triple-negative breast cancer cells. Sci. Signal *6*, ra66.

Mills, K.L., Gomes, A.M., Standlee, C.R., Rojo, M.D., Carmeliet, P., Lin, Z., and Machado, H.L. (2018). Gas6 is dispensable for pubertal mammary gland development. PLoS One *13*, e0208550.

Nieto, M.A., Huang, R.Y., Jackson, R.A., and Thiery, J.P. (2016). Emt: 2016. Cell *166*, 21–45.

Pal, B., Bouras, T., Shi, W., Vaillant, F., Sheridan, J.M., Fu, N., Breslin, K., Jiang, K., Ritchie, M.E., Young, M., et al. (2013). Global changes in the mammary epigenome are induced by hormonal cues and coordinated by Ezh2. Cell Rep. *3*, 411–426.

Pelissier, F., Claudet, I., Pelissier-Alicot, A.L., and Franchitto, N. (2014). Parental cannabis abuse and accidental intoxications in children: prevention by detecting neglectful situations and at-risk families. Pediatr. Emerg. Care *30*, 862–866.

Pelissier Vatter, F.A., Schapiro, D., Chang, H., Borowsky, A.D., Lee, J.K., Parvin, B., Stampfer, M.R., Labarge, M.A., Bodenmiller, B., and Lorens, J.B. (2018). High-dimensional phenotyping identifies age-emergent cells in human mammary epithelia. Cell Rep. *23*, 1205–1219.

Petersen, O.W., and Polyak, K. (2010). Stem cells in the human breast. Cold Spring Harb. Perspect. Biol. *2*, a003160.

Phillips, S., Prat, A., Sedic, M., Proia, T., Wronski, A., Mazumdar, S., Skibinski, A., Shirley, S.H., Perou, C.M., Gill, G., et al. (2014). Cell-state transitions regulated by SLUG are critical for tissue regeneration and tumor initiation. Stem Cell Rep. *2*, 633–647.

Qiu, P., Simonds, E.F., Bendall, S.C., Gibbs, K.D., Jr., Bruggner, R.V., Linderman, M.D., Sachs, K., Nolan, G.P., and Plevritis, S.K. (2011). Extracting a cellular hierarchy from high-dimensional cytometry data with SPADE. Nat. Biotechnol. *29*, 886–891.

Rios, A.C., Fu, N.Y., Lindeman, G.J., and Visvader, J.E. (2014). In situ identification of bipotent stem cells in the mammary gland. Nature *506*, 322–327.

Sandahl, M., Hunter, D.M., Strunk, K.E., Earp, H.S., and Cook, R.S. (2010). Epithelial cell-directed efferocytosis in the post-partum mammary gland is necessary for tissue homeostasis and future lactation. BMC Dev. Biol. *10*, 122.

Shackleton, M., Vaillant, F., Simpson, K.J., Stingl, J., Smyth, G.K., Asselin-Labat, M.L., Wu, L., Lindeman, G.J., and Visvader, J.E. (2006). Generation of a functional mammary gland from a single stem cell. Nature *439*, 84–88.

Shimono, Y., Zabala, M., Cho, R.W., Lobo, N., Dalerba, P., Qian, D., Diehn, M., Liu, H., Panula, S.P., Chiao, E., et al. (2009). Downregulation of miRNA-200c links breast cancer stem cells with normal stem cells. Cell *138*, 592–603.

Spike, B.T., Engle, D.D., Lin, J.C., Cheung, S.K., La, J., and Wahl, G.M. (2012). A mammary stem cell population identified and characterized in late embryogenesis reveals similarities to human breast cancer. Cell Stem Cell *10*, 183–197.

Stingl, J., Eirew, P., Ricketson, I., Shackleton, M., Vaillant, F., Choi, D., Li, H.I., and Eaves, C.J. (2006). Purification and unique properties of mammary epithelial stem cells. Nature *439*, 993–997.

Tan, T.Z., Miow, Q.H., Miki, Y., Noda, T., Mori, S., Huang, R.Y., and Thiery, J.P. (2014). Epithelial-mesenchymal transition spectrum quantification and its efficacy in deciphering survival and drug responses of cancer patients. EMBO Mol. Med. *6*, 1279–1293.

Terry, S., Abdou, A., Engelsen, A.S.T., Buart, S., Dessen, P., Corgnac, S., Collares, D., Meurice, G., Gausdal, G., Baud, V., et al. (2019). AXL targeting overcomes human lung cancer cell resistance to NK- and CTL-mediated cytotoxicity. Cancer Immunol. Res. *7*, 1789–1802.

Vaillant, F., Asselin-Labat, M.L., Shackleton, M., Forrest, N.C., Lindeman, G.J., and Visvader, J.E. (2008). The mammary progenitor marker CD61/beta3 integrin identifies cancer stem cells in mouse models of mammary tumorigenesis. Cancer Res. *68*, 7711–7717.

van Keymeulen, A., Rocha, A.S., Ousset, M., Beck, B., Bouvencourt, G., Rock, J., Sharma, N., Dekoninck, S., and Blanpain, C. (2011). Distinct stem cells contribute to mammary gland development and maintenance. Nature *479*, 189–193.

Villadsen, R., Fridriksdottir, A.J., Ronnov-Jessen, L., Gudjonsson, T., Rank, F., Labarge, M.A., Bissell, M.J., and Petersen, O.W. (2007). Evidence for a stem cell hierarchy in the adult human breast. J. Cell Biol. *177*, 87–101.

Visvader, J.E., and Stingl, J. (2014). Mammary stem cells and the differentiation hierarchy: current status and perspectives. Genes Dev. *28*, 1143–1158.

Vuoriluoto, K., Haugen, H., Kiviluoto, S., Mpindi, J.P., Nevo, J., Gjerdrum, C., Tiron, C., Lorens, J.B., and Ivaska, J. (2011). Vimentin regulates EMT induction by Slug and oncogenic H-Ras and migration by governing Axl expression in breast cancer. Oncogene *30*, 1436–1448.

Wuidart, A., Sifrim, A., Fioramonti, M., Matsumura, S., Brisebarre, A., Brown, D., Centonze, A., Dannau, A., Dubois, C., Van Keymeulen, A., et al. (2018). Early lineage segregation of multipotent embryonic mammary gland progenitors. Nat. Cell Biol. *20*, 666–676.

Ye, X., Tam, W.L., Shibue, T., Kaygusuz, Y., Reinhardt, F., Ng Eaton, E., and Weinberg, R.A. (2015). Distinct EMT programs control normal mammary stem cells and tumour-initiating cells. Nature *525*, 256–260.

Zhang, Z., Lee, J.C., Lin, L., Olivas, V., Au, V., Laframboise, T., Abdel-Rahman, M., Wang, X., Levine, A.D., Rho, J.K., et al. (2012). Activation of the AXL kinase causes resistance to EGFR-targeted therapy in lung cancer. Nat. Genet. *44*, 852–860.

iScience, Volume *23*

Supplemental Information

AXL Is a Driver of Stemness in Normal Mammary Gland and Breast Cancer

Agnete S.T. Engelsen, Katarzyna Wnuk-Lipinska, Sebastien Bougnaud, Fanny A. Pelissier Vatter, Crina Tiron, René Villadsen, Masaru Miyano, Maria L. Lotsberg, Noëlly Madeleine, Pouda Panahandeh, Sushil Dhakal, Tuan Zea Tan, Stacey D'mello Peters, Sturla Grøndal, Sura M. Aziz, Silje Nord, Lars Herfindal, Martha R. Stampfer, Therese Sørlie, Rolf A. Brekken, Oddbjørn Straume, Nils Halberg, Gro Gausdal, Jean Paul Thiery, Lars A. Akslen, Ole W. Petersen, Mark A. LaBarge, and James B. Lorens

Table S1. A unique 70-gene AXL MaSC gene signature

Mu Gene	Dir	Illumina ID	*Hu* Gene
Axl	1	ILMN_2651715	AXL
Supt3h	1	ILMN_1213872	SUPT3H
Elp2	1	ILMN_1216985	ELP2
Fbxo3	1	ILMN_1228298	FBXO3
Anp32a	1	ILMN_1230271	ANP32A
Selp	1	ILMN_1236889	SELP
Tmem154	1	ILMN_1237114	TMEM154
LOC100047935	1	ILMN_1239211	RPL5
Bhlhb9	1	ILMN_1251595	BHLHB9
Artn	1	ILMN_1254114	ARTN
Mrps12	1	ILMN_1254734	MRPS12
Aifm2	1	ILMN_1259418	AIFM2
Tnc	1	ILMN_2463180	TNC
Pbx2	1	ILMN_2599858	PBX2
Rab27a	1	ILMN_2614966	RAB27A
Oas1g	1	ILMN_2628822	OAS1
Ing4	1	ILMN_2639665	ING4
Mrpl3	1	ILMN_2643264	MRPL3
P2ry1	1	ILMN_2684316	P2RY1
Arfgap1	1	ILMN_2700126	ARFGAP1
Fbxo32	1	ILMN_2715893	FBXO32
Ss18l1	1	ILMN_2726159	SS18L1
Cdc42ep3	1	ILMN_2733185	CDC42EP3
Coasy	1	ILMN_2741236	COASY
Chchd10	1	ILMN_2749037	CHCHD10
Asb2	1	ILMN_2765759	ASB2
Pxdn	1	ILMN_2828896	PXDN
Actg2	1	ILMN_2839313	ACTG2
B230339M05Rik	1	ILMN_2894574	RALGAPB
Atp2a3	1	ILMN_2900462	ATP2A3
Acta2	1	ILMN_2923445	ACTA2
Ubac2	1	ILMN_2949605	UBAC2
Ccrl1	1	ILMN_2983624	CCRL1
Trub2	1	ILMN_2983686	TRUB2
Tnrc18	1	ILMN_3003152	TNRC18
Stk4	1	ILMN_3004142	STK4
Dyrk1b	1	ILMN_3053158	DYRK1B
Fam173a	-1	ILMN_1215218	FAM173A
Apoe	-1	ILMN_1216042	APOE
Taf5	-1	ILMN_1218205	TAF5
Pcdh10	-1	ILMN_1228833	PCDH10
1500015O10Rik	-1	ILMN_1249000	C2orf40
Slc19a2	-1	ILMN_1250531	SLC19A2
Mal2	-1	ILMN_1252628	MAL2
Cdk5r1	-1	ILMN_1259339	CDK5R1
Akr1c18	-1	ILMN_1260323	AKR1C3
Tnfrsf12a	-1	ILMN_2424299	TNFRSF12A
Tmem2	-1	ILMN_2430220	TMEM2
Ccar1	-1	ILMN_2516266	CCAR1
Lmna	-1	ILMN_2597710	LMNA
Ell3	-1	ILMN_2627179	ELL3

Mu Gene	Dir	Illumina ID	*Hu* Gene
Hexim1	-1	ILMN_2631994	HEXIM1
Cdkn1a	-1	ILMN_2634083	CDKN1A
P2ry6	-1	ILMN_2663130	P2RY6
Ppp1r3c	-1	ILMN_2667091	PPP1R3C
2200001I15Rik	-1	ILMN_2678637	FAM25A
Hbegf	-1	ILMN_2698449	HBEGF
Nanos1	-1	ILMN_2701355	NANOS1
Rpusd4	-1	ILMN_2718974	RPUSD4
Fnip1	-1	ILMN_2725155	FNIP1
Rrp12	-1	ILMN_2728118	RRP12
Snap29	-1	ILMN_2730767	SNAP29
Tec	-1	ILMN_2752933	TEC
Fosb	-1	ILMN_2778279	FOSB
Wif1	-1	ILMN_2857748	WIF1
Rps2	-1	ILMN_2946616	RPS2
Arhgap20	-1	ILMN_2959729	ARHGAP20
Fhl1	-1	ILMN_3117381	FHL1
Lif	-1	ILMN_3137287	LIF
Sfrs5	-1	ILMN_3148662	SRSF5

Figure S1. Controls for RNA *in situ* experiments

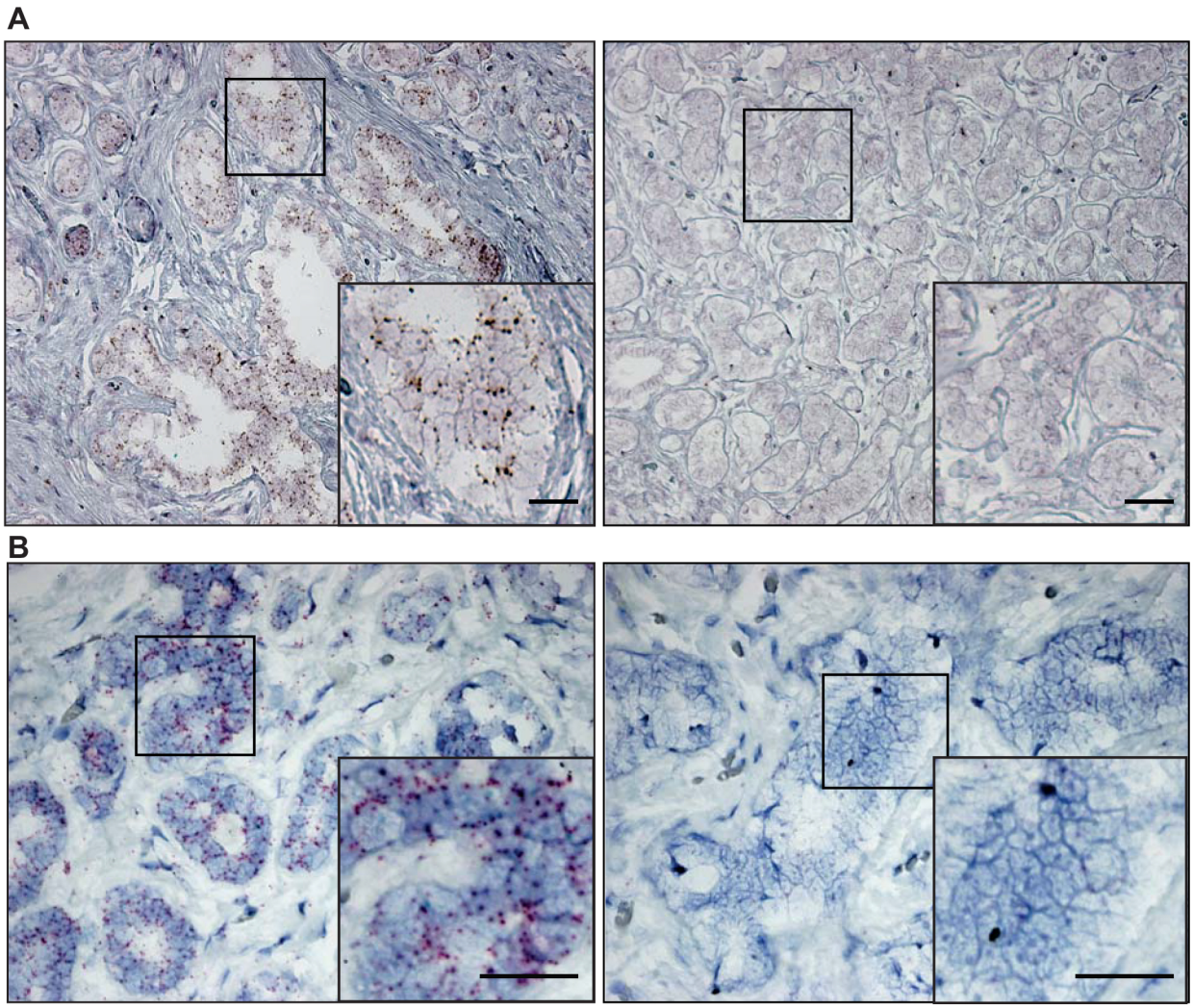

Figure S2. Description of the AXL-targeting mutation in B6.129P2-*Axltm1Dgen/J* mice

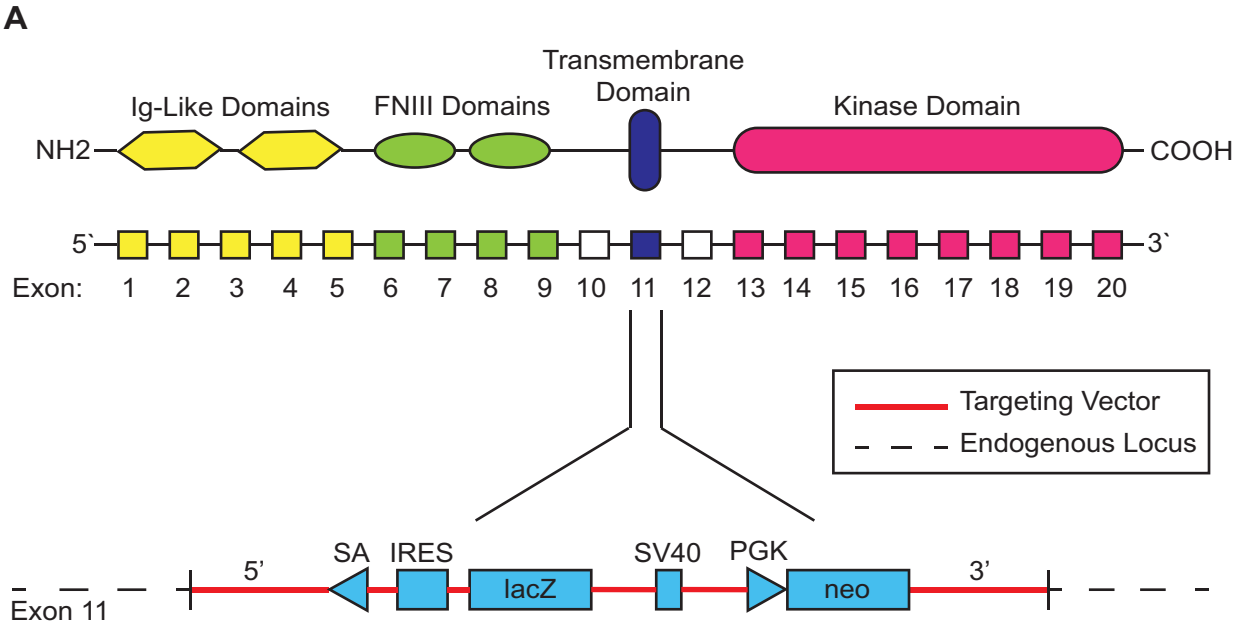

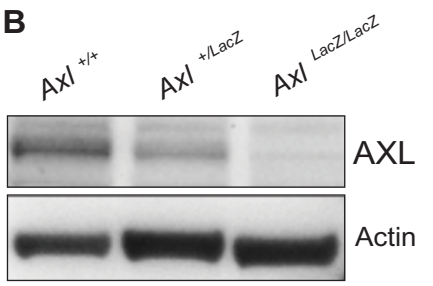

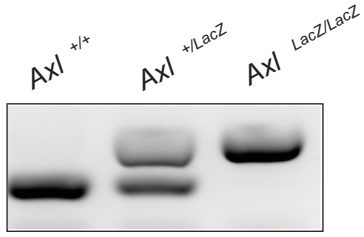

Figure S3. Characterization of AXL null mammary glands

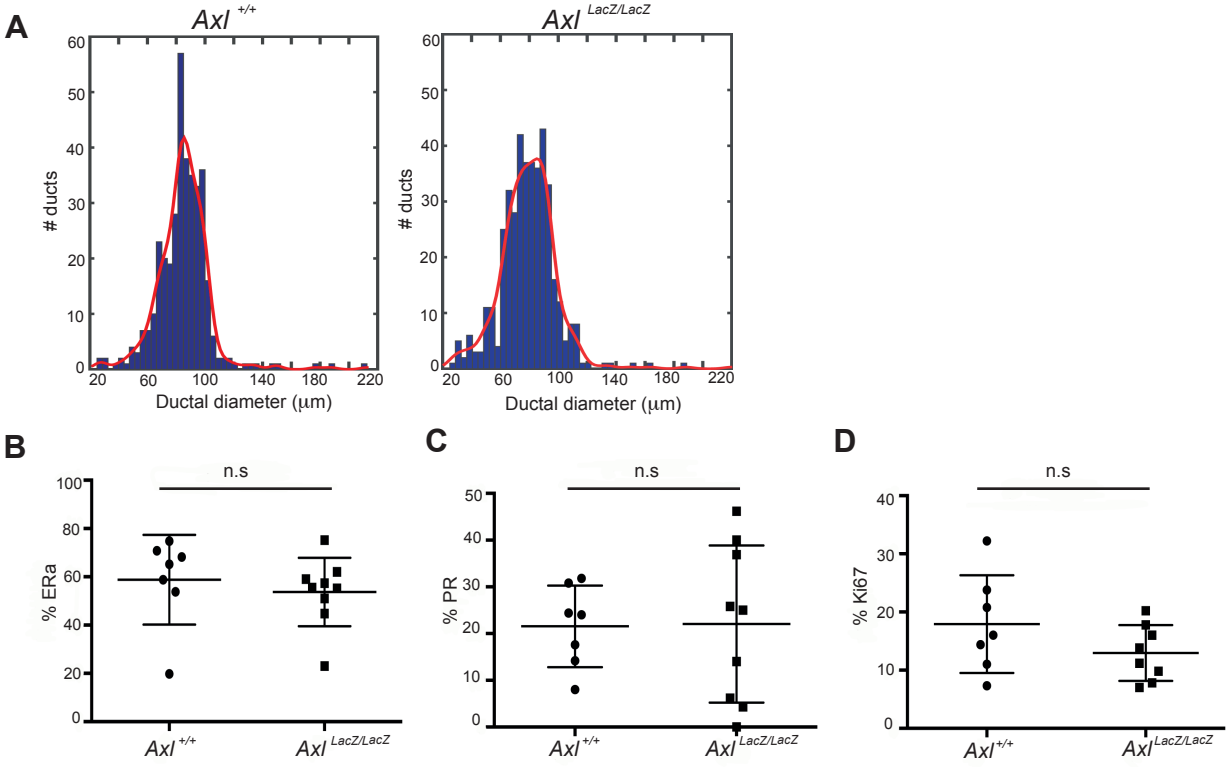

Figure S4. Analysis of mammary gland whole mounts from pubescent warfarin-treated mice

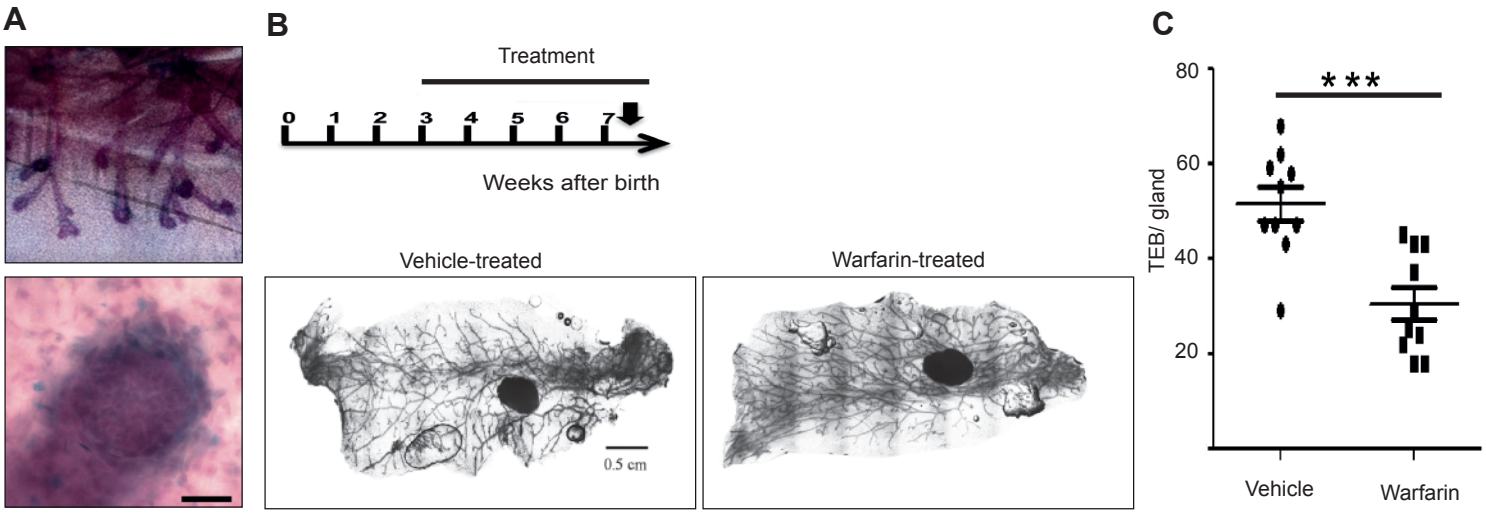

Figure S5. The AXL-stem gene expression signature is elevated in basal-like tumors in the Metabric breast cancer patient cohort

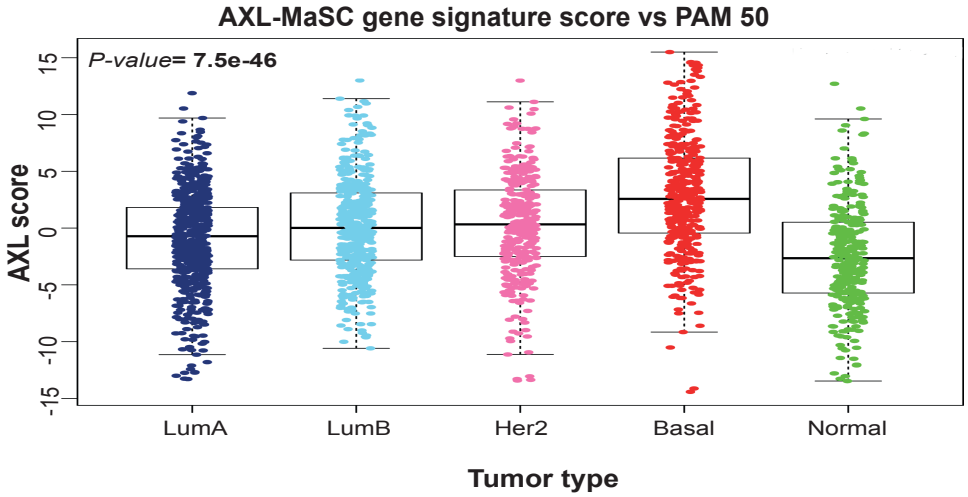

Figure S6. AXL overexpression is not sufficient to induce EMT in MCF10a cells

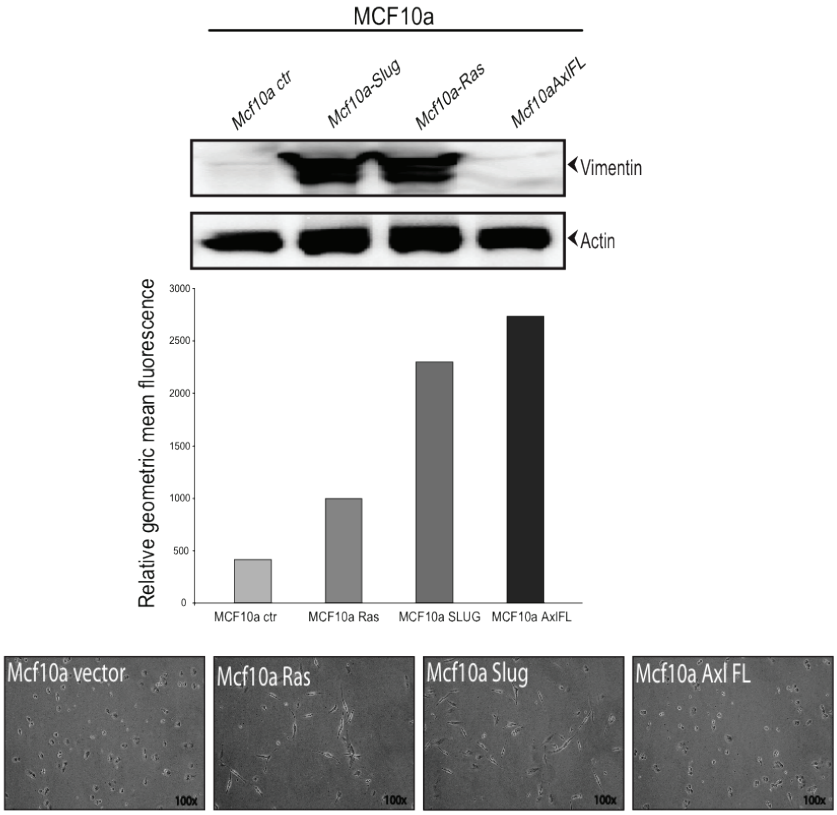

Figure S7. AXL is required for Slug-mediated epithelial plasticity

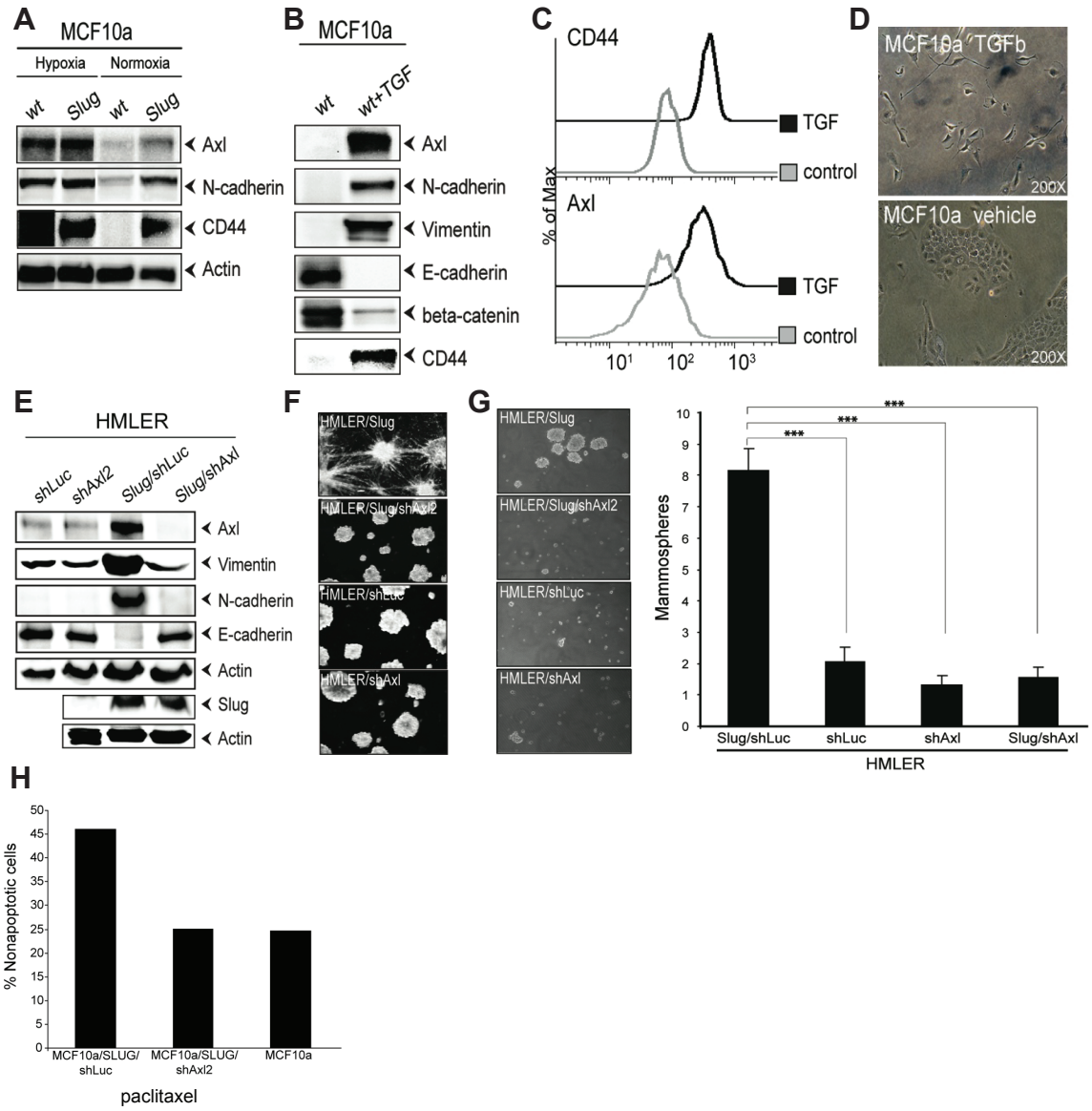

Figure S8. Deregulated signaling pathways of AXL null WNT induced tumors

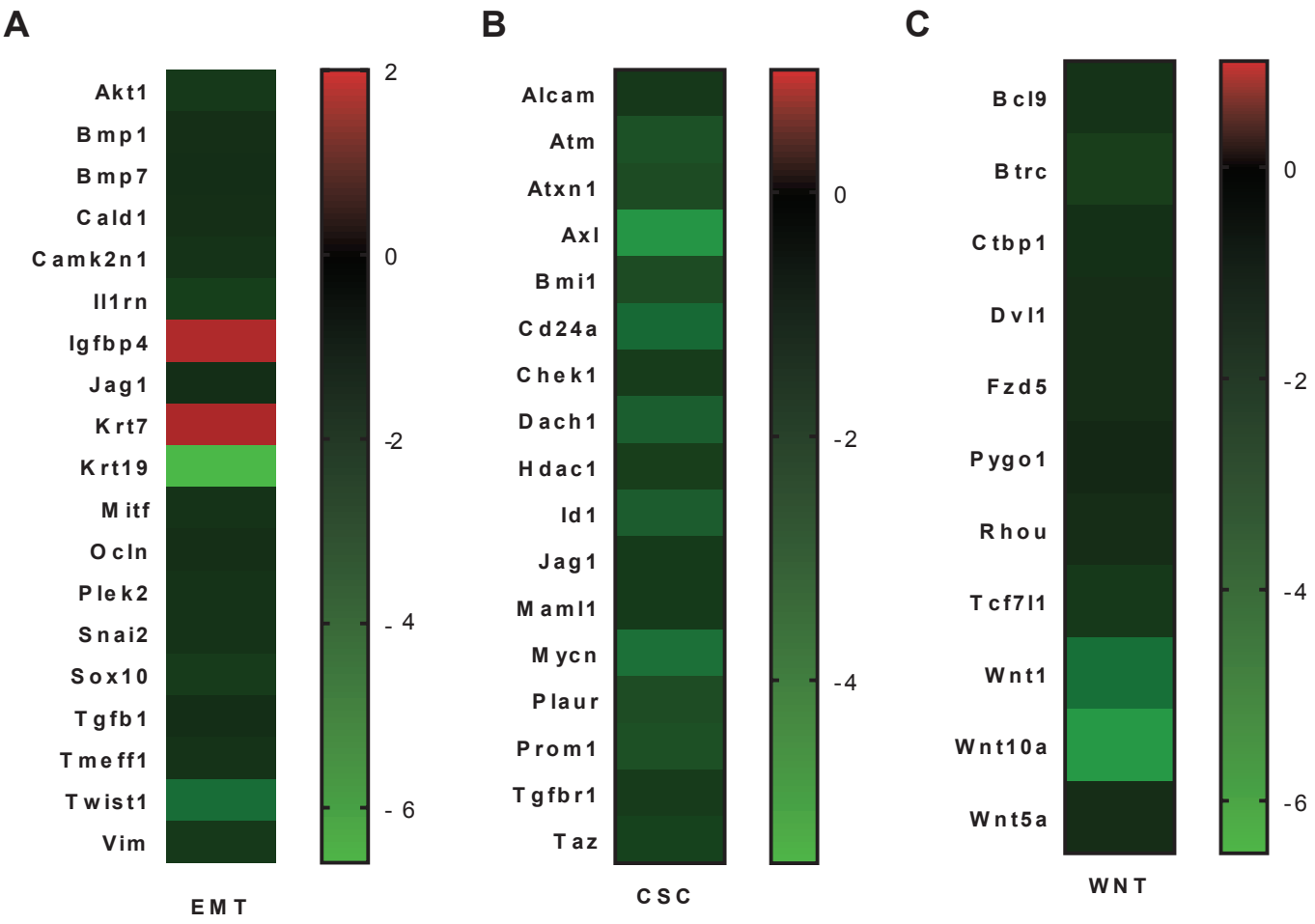

Supplemental Table and Figure Legends

Table S1. A unique 70-gene AXL MaSC gene signature (related to Figure 5A-B, Figure 6A-C)
The top 70 differentially expressed genes (33 down-regulated and 37 up-regulated by rank product test) determined by Illumina MouseWG-6 v2.0 Expression BeadChip Array gene expression analysis of mRNA isolated from FACS-sorted FDG^{high} $AXL^{+/LacZ}$ and FDG^{high} $AXL^{LacZ/LacZ}$ cell populations. Mu=murine, Hu= human. Dir= direction (1=up, -1=down).

Figure S1. Controls for RNA *in situ* experiment (related to Figure 1 J-N)
(A) Appropriate controls for RNA in situ experiment for single RNA in situ approach with chromogen DAB (brown). Left image shows positive control probe targeting the housekeeping gene PPIB, and right image shows the negative control probe targeting the bacterial DapB gene. Counterstain hematoxylin. (B) Appropriate controls for the dual RNA in situ approach. Left image shows positive control probes targeting the housekeeping gene PPIB (C2: chromogens AP-based Fast Red), as well as POLR2A (C1: chromogen HRP-based green) for the dual approach. Right image show hybridization with negative control probes targeting the bacterial gene DapB, each detection channel (C1 and C2) has its own negative control probe, Counterstain hematoxylin. Scalebar 50 μm.

Figure S2. Description of the AXL-targeting mutation in B6.129P2-*AXL*$^{tm1Dgen/J}$ mice (related to mice described in Figure 4. Gene signatures derived from these mice are further described in Table S1, Figure 5 and Figure 6. These mice has been crossed with MMTV-Wnt1 mice as shown in Figure 7I-J)
(A) Schematic illustration of the *LacZ-Neo* cassette insertion site in exon 11 of the murine AXL gene, disrupting AXL protein expression. A 5' splice acceptor ensures that the LacZ open reading frame is spliced into the endogenous AXL mRNA under control of the murine AXL promoter. (B) Western blot analysis of murine AXL expression in dissociated lung tissue from wildtype ($AXL^{+/+}$), heterozygous ($AXL^{+/LacZ}$), and homozygous ($AXL^{LacZ/LacZ}$) mice of the B6.129P2-$AXL^{tm1Dgen}$/J strain (The Jackson Laboratory, Bar Harbour, ME). AXL protein expression from *LacZ*-insertion allele is undetectable. (C) PCR product (http://jaxmice.jax.org/protocolsdb/) from different genotypes of B6.129P2-$AXL^{tm1Dgen}$/J mice (wildtype ($AXL^{+/+}$), heterozygous ($AXL^{+/LacZ}$), and homozygous ($AXL^{LacZ/LacZ}$). Larger sized band represents *LacZ*-insertion allele.

Figure S3. Characterization of AXL null mammary glands (related to Figure 4 A-C)
(A) Mammary gland whole-mounts from adult (16 week-old) $AXL^{+/+}$ (wildtype) and $AXL^{LacZ/LacZ}$ (*AXL*-null) mice were harvested and processed for characterization by carmine alum staining. Ductal diameters were quantified with MATLAB using image segmentation analysis of the carmine-alum stained glands. The Kolmogorov–Smirnov test rejected the hypothesis that ductal diameters of wildtype $AXL^{+/+}$and $AXL^{LacZ/LacZ}$ are derived from the same distribution (p= 9.23x10-7). (B-D) Histopathologic quantification of (B) ERα, (p= 0.35), (C) PR (p= 0.96) and (D) Ki67, (p= 0.24) immunohistochemistry of mammary duct FFPE tissue sections of adult AXL+/+ (wildtype) $AXL^{LacZ/LacZ}$ mammary glands. n.s= non-significant by Mann-Whitney, non-parametric test.

Figure S4. Analysis of mammary gland whole mounts from pubescent warfarin-treated mice (related to Figure 5E)
(A) β-galactosidase activity is shown in terminal end buds (TEB) of mammary gland whole-mounts of 6-week old prepubescent $AXL^{+/LacZ}$ mice stained by β-galactosidase histochemistry and counterstain by carmine alum. β-galactosidase activity was prominent in cells located to the cap region of TEBs. Scalebar: 100μm. (B) Schematic overview of warfarin treatment regimen. Peroral warfarin administration were initiated at in 3 week-old mice post-weaning. Representative composite images of carmine alum stained mammary gland whole-mounts from mice treated for 5 weeks with either pure or warfarin (1 mg/L) containing drinking water. (C) Quantification of terminal end buds (TEB) in carmine alum stained mammary gland whole mounts harvested from 8 week-old control and warfarin treated animals (t-test, p=0.0004). Duration of treatment: 5 weeks.

Figure S5. The AXL-stem gene expression signature is elevated in basal-like tumors in the Metabric breast cancer patient cohort (related to Figure 6C)
The Metabric breast cancer patient cohort (n=1,980) (Curtis et al., 2012) was interrogated with the AXL MaSC gene expression signature (AXL-stem, Table S1) to assess the influence of the novel AXL stem gene expression signature on clinical endpoints. The AXL-stem score correlated with tumor subtype of PAM50 subtyped tumors is shown; the AXL score is significantly elevated in the basal-like tumors (P = 7.5x10-46, Kruskal-Wallis rank test).

Figure S6. AXL overexpression is not sufficient to induce EMT in MCF10a cells (related to Figure 7 A-D)
MCF10a cells transduced with control vector or retroviral expression vector encoding AXL, Slug or Ha-Ras(G12V) as well as GFP reporter-gene. Post transduction, cells were FACS sorted based on their GFP expression, and protein expression of Vimentin were measured by Western blotting (upper). Cell-surface expression of AXL were quantified by flow cytometry (middle) (>100,000 events) and displayed as geometric mean. Phase contrast images displaying cell morphologies of control and AXL-, Slug- and Ha-Ras(G12V)-expressing MCF10a cells are shown below.

Figure S7. AXL is required for Slug-mediated epithelial plasticity (related to Figure 7 A-F)
(A) AXL is induced by hypoxia. Western blot analysis of CD44, N-cadherin (CDH2), and AXL protein expression in MCF10a/control and MCF10a/Slug cells grown under normoxic and hypoxic (1% O2) conditions. (B) AXL is induced by TGFb. Western blot analysis of AXL, CD44, epithelial (E-cadherin, ß-catenin) and mesenchymal (vimentin, N-cadherin) marker expression. (C) Flow cytometric analysis of CD44 and AXL surface levels; and (D) Phase contrast images of MCF10a cell morphology, after culture with TGFb (10 ng/ml) or vehicle for 7 days. (E) AXL is required for Slug-mediated mesenchymal and stem cell traits in HMLER cells. HMLER transduced with control or Slug retroviral expression vectors (with GFP reporter gene), as well as AXL-targeting shRNA (shAXL2) or control luciferase shRNA (shLuc) vectors (with RFP reporter gene), were sorted for GFP and RFP, and analyzed for by western blot for expression of AXL, Slug (SNAI2), epithelial (E-cadherin, β -catenin) and mesenchymal (vimentin, N-cadherin). β-actin was used as a loading control. (F) AXL is required for EMT-induced stellate colony formation. Phase contrast images of HMLER/shLuc, HMLER/shAXL2 and HMLER/Slug/shAXL2 and HMLER/Slug/shLuc cell colonies in 3D embedded lrECM (matrigel). (G) AXL is necessary for EMT-induced mammosphere formation. Quantification of mammosphere formed by HMLER/shLuc, HMLER/shAXL2 and HMLER/Slug/shAXL2 and HMLER/Slug/shLuc cells. Y-axis represents total number of mammospheres formed per well (mean ±S.D., n= 6; *** p<0.0001, t-test). (H) AXL signaling is required for EMT-induced drug resistance. Multicolor flow cytometry analysis of MCF10a cells transduced with control or Slug retroviral vector following 24 hour treatment with paciltaxel (30 µg/ml). The percentage of non-apoptotic cells represents the % viable cells post-treatment (of >100,000 total events) within the AnnexinV negative, Sytox Blue negative gate for each cell line.

Figure S8. Deregulated signaling pathways of AXL null WNT induced tumors (related to Figure 7 I-K)
Pathway focused RT2 Profiler TM PCR arrays demonstrate alterations in (A) EMT signaling pathway, (B) CSC pathway and (C) WNT pathway analysed in 6 $Axl^{+/+}$ wild-type and 4 $AXL^{LacZ/LacZ}$ (*Axl*-null) *Wnt1*- induced tumors. The gene expression levels of the *Axl*-null (n=4) samples were quantified relative to the expression levels for WT samples (n=6) after normalization to the levels of the suitable housekeeping genes (ACTB, B2M, GAPDH, GUSB, HSP90AB1) in the panel. Data in heatmaps are reported as mean fold changes.

Transparent Methods

Reagents

Anti-hAXL MAB10C9 (Lorens laboratory), MAB154, AF154 (R&D Systems), Anti-mAXL (sc-1097, Santa Cruz), mouse anti-human Slug (L40Cb, Cell Signaling), rabbit anti-human E-cadherin (24E10, Cell Signaling), rabbit anti-human N-cadherin (ab18203, Abcam), α-actin (A5060, Sigma), mouse anti-human β-catenin (L54E2, Cell Signaling), rabbit anti-human β-catenin (Cell Signaling), mouse rat anti-human Vimentin (MAB2105, R&D Systems), anti-CD227-FITC (Becton Dickinson, clone HMPV), anti-CD10-PE (BioLegend, clone HI10a), anti-CD117- Alexa647 (BioLegend, clone 104D2), EPCAM-BV421 (BioLegend, clone 9C4), anti-CD49f-PE (Chemicon, clone CBL-458P), anti-K14 (Covance, polyclonal rabbit), anti-K19 (Developmental Studies Hybridoma Bank, clones Troma-II and Troma-III), anti-CD44 (Cell Signaling, 3570), anti-CD31-PE (17-0311), anti-CD45-PE (17-0451), and anti-CD11b (11-0112; eBioscience). Imatinib (LC laboratories I-5508) and bemcentinib (also known as BGB324 and R428, BerGenBio AS) (Holland et al., 2010) were prepared in DMSO.

Immunohistochemistry (IHC-P, IHC-F)

IHC-P, fluorescent detection: Paraffin-embedded normal human breast tissue sections (generously provided by Dr. A. Borowsky) were prepared for immunofluorescence and stained as previously described (Garbe et al., 2012) using anti-K14 (Covance, polyclonal rabbit), anti-K19 (Developmental Studies Hybridoma Bank, clone Troma-III), anti-CD117 (BioLegend, clone 104D2), anti-hAXL MAB10C9 (BerGenBio ASA) overnight at 4oC, visualized with fluorescent secondary antibodies (Invitrogen) and 4,6-diamidino-2-phenylindole (DAPI) nuclear stain at room temperature for 1 hour, and imaged using a 710LSM microscope (Carl Zeiss).

IHC-P, chromogenic detection: Paraffin-embedded normal human breast tissue sections were prepared for staining as described (Garbe et al., 2012). Anti-Axl antibody were incubated o/n at 1:6000 dilution (clone EPR19880, Abcam). Peroxidase stain was performed by Ultravision ONE Destection System (Thermo Scientific). Sections were counterstained with hematoxylin and mounted with Entellan (Merck) prior to imaging.

IHC-F: Mammary tissue specimens were embedded in OCT and snap frozen in liquid nitrogen. Cryosections (6µm thickness) were stained with anti-Axl antibody (clone EPR19880, 1:100, Abcam); anti-K14 (clone LL002, 1:100, Monosan); anti-K19 (clone A53-B/A2, 1:100, BioLegend). Alexa Fluor conjugated secondary antibodies (1:500, Invitrogen) and 4,6-diamidino-2-phenylindole (DAPI) nuclear stain.

RNA *in situ* hybridization

In situ detection of *AXL* and *GAS6* mRNA in human mammary FFPE tissue were performed using the RNA Scope technology. Probes and reagents were provided by Advanced Cell Diagnostics (ACD, Hayward, CA). Briefly, human archival mammary gland tissue sections of 5 um thickness were deparaffinized in xylene, followed by dehydration in ethanol. Tissue sections were then incubated in citrate buffer (10 nM/ L, pH 6) maintained at boiling temperature (100oC to 103^{o}C) using a hot plate for 15 minutes, rinsed in deionized water, and immediately treated with 10 µg/ mL protease (Sigma-Aldrich, St. Louis, MO) at 40oC for 30 minutes in a HybEZ hybridization oven (Advanced Cell Diagnostics, Hayward, CA). Hybridization with target probes, preamplifier, amplifier, label probe and chromogenic detection were performed according to ACD's recommendations. Sections were counterstained with hematoxylin and mounted with EcoMount prior to imaging. Assays using archival FFPE specimens were performed in parallel with positive and negative control probes, to ensure interpretable results (Supplementary Figure 4). Histo score analysis were performed to evaluate the heterogeneity in marker expression. Cells were scored and grouped in 5 bins based on the number of dots/ cell (Bin 0= 0 dots/cell, Bin 1= 1-3 dots/ cell, Bin 2= 4-9 dots/ cell, Bin 3= 10-15 dots/cell (<10% dots in clusters), Bin 4= >15 dots/cell (>10% dots in clusters). Each sample was manually scored, and the percentage of cells in each bin recorded. Histo score was calculated by totaling the percentage of cells in each bin according to the given formula. Histo score= 0*(% of cells in bin 0) +1*(% of cells in bin 1) +2*(%of cells in bin 2) +3*(% of cells in bin 3) +4*(% of cells in bin 4). Histo score is provided on the range 0-400.

Human mammary epithelial cells (HMEC) isolation and culture
Pre-stasis human mammary epithelial cells (HMEC) were derived from reduction mammoplasties (n=60) were established and maintained as described (Labarge et al., 2013) in low-stress M87A medium with oxytocin and cholera toxin (Garbe et al., 2012). HMEC of 4th passage or lower were used.

Flow cytometry and FACS sorting
Flow cytometry analysis of MCF10a cells was conducted as described (Gjerdrum et al., 2010). For flow analysis of isolated human breast epithelial organoids and pre-stasis HMEC, cells were recovered following trypsin treatment and resuspended in their media. For enrichment or identification of luminal epithelial and myoepithelial lineages, anti-CD227-FITC (Becton Dickinson, clone HMPV, 1:50) or anti-CD10-PE, -PE-Cy5 or -APC (BioLegend, clone HI10a, 1:50), were used, respectively. Other analysis was carried out with EPCAM-BV421 (BioLegend, clone 9C4), anti-CD49f-PE (Chemicon, clone CBL-458P, 1:50), anti-CD117-Alexa647 (BioLegend, clone 104D2, 1:200) and anti-hAXL MAB10C9 conjugated to Alexa-647 (1:200). MABs were added to the media at 1:50 for 25 minutes on ice, washed in PBS, and sorted or analyzed. KIT-expressing HMEC progenitors were isolated by staining with anti-CD117-PE (BioLegend, clone 104D2, 1:200) and were added to cells in media for 25 min on ice, washed in PBS and sorted on a FACS Vantage SE DIVA (Becton Dickinson). β -galactosidase flow cytometry was done using FluoReporter® lacZ Flow Cytometry Kit (Molecular Probes F-1930). For transplantation assays and organoid assays of murine cells the following sorting strategy were used: freshly dissociated and labeled cells were discriminated from the debris and gated in the forward scatter (FSC-A) and side scatter (SSC-A) plots. Subsequently, the forward scatter Width (FSC-W) versus FSC-A plots were used for doublet cell exclusion. Propidium iodide (PI) staining was used for dead cell discrimination and the APC channel was used as a dump channel for the APC conjugated lineage markers used. Thus, only single, viable, PI-negative, and APC-negative cells were included in the final sort of FDG-high and FDG-low cells used for subsequent experiments. A post-sort analysis was performed to verify purity of the sorted cells and sort numbers were obtained from each sort, however, the cell counts used for subsequent experiments were determined by visualizing and enumerating live healthy single cells. T Data analysis was carried out on 500 000 events using the FlowJo software (Tree Star, Inc., Ashland, OR, USA). SPADE analysis was performed with Cytoscape (www.cytoscape.org) and R (Foundation for Statistical Computing).

High-dimensional Mass cytometry
Mass cytometry analysis of dissociated primary human breast epithelia was described in great detail in (Pelissier Vatter et al., 2018). Primary HMEC strains were generated and maintained as described (Labarge et al., 2013). All tissues were obtained with proper oversight from the Lawrence Berkeley National Laboratory institutional review board. Breast tissue from reduction mammoplasty was manually dissected to enrich for gland-containing material. Stromal tissue was separated from epithelial fragments using a brief treatment with collagenase. The uncultured breast epithelia samples were dissociated as single cells with trypsin. Cells were incubated with cisplatin (WR International, Cat# 89150- 634, 25 mM) for 1 min to assess cell viability (Fienberg et al., 2012), fixed in 1.6% PFA for 10 min at RT, and washed once with Cell Staining Media (CSM, PBS with 0.5% BSA and 0.02% NaN3 with 0.03% saponin). The cells were then resuspended in PBS, and DMSO stocks of the barcoding reagent were added as described (Bodenmiller et al., 2012, Zivanovic et al., 2014). The cells were incubated at RT for 30 min, washed three times with CSM, and then pooled into a single FACS tube for staining with metal-labeled antibodies for 1 hr at RT. After antibody staining, the cells were washed twice with CSM and once with PBS, and then incubated for 20 min at RT or overnight at 4°C with an iridium-containing intercalator (DVS Sciences) in PBS with 1.6% PFA. The cells were then washed three times with CSM and once with PBS, diluted with water to ~106 cells/mL, and filtered through a 40-mm membrane just before analysis by mass cytometry. The scale used before analysis is the arcsinh with the cofactor of 5 (x_transf = asinh(x/5)). After gating out viable and iridium-labeled events, the data were analyzed by applying tSNE. This non-linear dimensionally reduction technique is implemented via Barnes-Hut approximations in the MATLAB toolbox cyt (Amir el et al., 2013). We used the default parameters (initial dimensions, 110; perplexity, 30; and theta, 0.5). The

unsupervised PhenoGraph algorithm in cyt has been used to group cells that are phenotypically similar and cluster these subpopulations using modularity optimization (Levine et al., 2015). tSNE and PhenoGraph were performed only on surface markers. A number of neighbors of 800 was selected. The heatmap was obtained with MATLAB. The accession number for the CyTOF data reported in this paper is Mendeley Data: https://doi.org/10.17632/j7mrbgt3hh.1.

3D-embedded laminin-rich ECM assay
MCF10a or KIT-enriched HMEC were resuspended in media (50000 cells/ µL) and 200 µL of matrigel (BD Sciences 356234) were added to the cells and transferred to a 24-well plate pre-coated with 50 µL of Matrigel, then cultured for 10-12 days prior to microscopy analysis. For immunofluorescence analysis of HMEC colonies, Matrigel smears were fixed in methanol/acetone 1:1 at -20°C for 20 min, incubated with blocking buffer overnight at 4°C, incubated with anti-K14 and anti-K19 overnight at 4°C, extensively washed with PBS, then incubated with fluorescent secondary antibodies overnight at 4°C, and washed overnight at 4°C before mounting coverslips with Fluormount G. Insert Keratin 5 (murine).

Mammosphere formation assay
Mammosphere culture of MCF10a was performed as previously described(Dontu et al., 2003). Single cells were plated in ultra-low attachment plates (Corning, Acton, MA, USA) 20,000 viable cells/ ml. For mammosphere assays of HMEC, flow cytometry sorted KIT+ enriched HMEC (p4) were resuspended in mammosphere media (MammoCult human medium kit (StemCell 05620, enriched with heparin and hydrocortisone) at 25,000 cells/ mL in polyHema (0.133 mL at 12 mg/ ml in 95% EtOH) treated 24-well plates (in triplicate) and cultured for 10 days. Large (≥70 µm) and hollow mammospheres were identified by microscopy of each well. Total mammospheres per well were quantified using ImageJ. Secondary mammospheres were prepared by trypsinizing and resuspending for cell from first passage mammospheres. For the immunofluorescence, mammospheres were fixed in 4% paraformaldehyde for 5 min, blocked with PBS, 5% normal goat serum, 0.1% Triton X-100, and incubated with anti-K14 (1:1000, Covance, polyclonal) and anti-K19 (1:10, Developmental Studies Hybridoma Bank, clone Troma-III) overnight at 4°C, then visualized with fluorescent secondary antibodies (Invitrogen) incubated with sections for 2 hours at room temperature.

Gene expression analysis
Global gene expression analysis of HMEC lineage was performed on FACS sorted (FACS Vantage SE DIVA, Becton Dickinson) pre-stasis HMEC strains 240L and 122L cells (4th passage). Total RNA from FACS-enriched primary culture cells was isolated with TRIzol (Invitrogen) and RNeasy Mini column (Qiagen) and evaluated using Bioanalyzer (Agilent Technologies). Gene expression levels were measured using the Illumina HumanHT-12 v4 Expression BeadChip whole-genome expression array. The Illumina Bead Array data were quality controlled in Genome Studio and both probe level and gene level data were imported into J-Express Pro (http://jexpress.bioinfo.no) for analysis. After quantile normalization both datasets were log2 transformed. Correspondence Analysis (Fellenberg et al., 2001) was performed on the datasets, together with Hierarchical Clustering of the samples using a Pearson correlation measure on a per gene mean centered version of the data.

Gene expression analysis of FDG FACS-sorted 16 week old nulliparous $AXL^{+/LacZ}$ and $AXL^{LacZ/LacZ}$ (B6.129P2-$AXL^{tm1Dgen}$ strain, Jackson Labs) was conducted using the Illumina MouseWG-6 v2.0 Expression BeadChip (BD-201-0202, BD-201-0602). Log2 quantile normalized of the gene expression data were used for unsupervised hierarchical clustering, gene signature analysis and differentially expressed genes. Hierarchical clustering was performed using Pearson's correlation as distance measurement. Gene signatures among cell population were determined by comparing the gene expression levels and available molecular signatures of the mammary cell subpopulations (Lim et al., 2009) using GSEA software package (Subramanian et al., 2005). Differentially expressed genes between $AXL^{+/LacZ}$ FDG^{high} and $AXL^{LacZ/LacZ}$ FDG^{high} cell groups were identified using Rank Product method. The genes with a p-value <0.01 and fold change >= 1.5 were considered as differentially expressed genes. All analyses were performed using R version 3.2.2. To assess the influence of AXL and its downstream targets on survival of breast cancer patients, we

derived a score capturing the expression of these genes. The score is the sum of the top 70 genes from the rank product test, of which 33 genes were downregulated and 37 upregulated, adjusted for expected directionality. For genes represented by multiple probes, mean signal intensity was used. The influence on breast cancer-specific survival and putative difference between molecular subtypes were investigated in the Metabric cohort, composed of 1980 breast cancer patients enrolled at five different hospitals in the UK and Canada (Curtis et al., 2012). Gene expression was assessed using the Illumina HT-12 v3 microarray and normalized data was downloaded from the European Genome-phenome Archive (EGA) data portal. Missing values were imputed using the impute.knn function as implemented in the R library 'impute' with default settings (R package version 1.46.0.). The data was batch adjusted for hospital effect using the pamr.batchadjust function in the 'pamr' library with default settings. Association between the score and molecular subtypes was tested using Kruskal-Wallis rank test, and correlations were estimated with Spearman's rank correlation. Survival analyses were performed using Cox proportional hazards regression model as implemented in the R library 'rms'. The generic EMT 315 gene expression signature were used to compute the EMT score of the FDG high $Axl^{+/LacZ}$ and $Axl^{LacZ/\ LacZ}$ populations as previously described (Tan et al., 2014).

MMTV-Wnt1 mammary tumor cells (6 from *MMTV-Wnt1:Axl*$^{+/+}$ and 4 from *MMTV-Wnt1:Axl*$^{+/LacZ}$) were analyzed using RT2 Profiler TM PCR arrays (96 X 4) (Mouse WNT signaling pathway PAMM-043ZG-4; Mouse Epithelial to Mesenchymal Transition PAMM-090ZG-4 ; Mouse Cancer Stem cells PAMM-176ZG-4, Qiagen) as per the manufacturer's guidelines. The tumors were harvested from mice and flash frozen for RNA isolation. Total RNA extraction was performed using RNeasy Mini Kit (Qiagen), and cDNA was synthesized for RT-qPCR using the RT2 first strand kit (Qiagen) as recommended by the manufacturer. RT-qPCR was performed on a LightCycler® 480 (Roche) using RT² SYBR Green qPCR Mastermix (Qiagen) for SYBR Green detection of each reaction and expression levels were determined using the ΔΔCt method. Expression levels were normalized to housekeeping genes (ACTB, B2M, GAPDH, GUSB, HSP90AB1) with small changes in their expression across different sample groups (differences in CT values less than 1). The p values were calculated based on a Student's t-test (unpaired; *P<0.05, **P<0.01, ***P<0.001) from the 2-ΔΔCT values obtained for each gene in the WT group and KO groups.

Retroviral vectors
MCF10a (American Type Culture Collection, Rockville, MD) were cultured as described (Gjerdrum et al., 2010). The CRU5-IRES-hSlug retroviral vector prepared as described (Gjerdrum et al., 2010). Retroviral production and infections were conducted using Phoenix A retroviral packaging cells as described (Swift et al., 2001).

Immunoblotting
MCF10A cells were lysed using NP40 Cell Lysis Buffer (40 mM HepesNAOH, 75 mM NaCl, 2 mM EDTA, 1% NP40, phosphatase inhibitor cocktail tablet, protease inhibitor cocktail tablet (Roche)). Running of SDS/PAGE gel and immunoblotting were carried out according to standard procedures.

Animal studies
Animal experiments were approved by the Institutional Animal Care Research Authority and in accordance with The European Convention for the Protection of Vertebrates Used for Scientific Purposes. Animals were housed in a germ-free environment in filter top cages. Environmental parameters were monitored by the Laboratory Animal Facility of UIB and followed the institutional SOP. Animals were provided certified laboratory feed and sterile drinking water ad libitum. Clinical observation of animal appearance were recorded daily. At study termination the animals were anesthetized by Sevoflurane and euthanized by cervical dislocation euthanized following Institutional SOP.

Mammary transplantation assay
Mammary glands were dissected from adult (12-16 week old) B6.129P2-*AXL*^{tm1Dgen} heterozygous and homozygous mice (Jackson Labs), washed in cold PBS, minced and incubated overnight at 37˚C in dissociation medium containing EpiCult-B Basal Mouse Medium (05611, STEMCELL Technologies) supplemented with 5% fetal bovine serum and

1.7 mg/ ml collagenase XI (C9697, Sigma). After dissociation and centrifugation, cells were suspended in a 1: 4 mixture of cold Hanks Balanced Salt Solution Modified (37250, STEMCELL Technologies) supplemented with 2% FBS and ammonium chloride (07850, STEMCELL Technologies) in order to lyse red blood cells. Dissociation was ended by proteolysis using pre-warmed 0.25% trypsin-EDTA followed by incubation in pre-warmed 5 mg/mL dispase with 0.1 mg/mL DNase I solution (07900, STEMCELL Technologies). FluoReporter® LacZ Flow Cytometry Kit (F-1930, Molecular Probes) was used for fluorescent β-galactosidase detection followed by FACS. Protocol provided by manufacturer was followed, with minor modifications. Briefly, isolated mammary epithelial cells were suspended in staining medium containing Hanks Balanced Salt Solution Modified (37250, STEMCELL Technologies) supplemented with 2% FBS and 300 µM chloroquine to inhibit lysosomal β-galactosidase activity. The same volumes of 2 mM FDG working solution and cell suspension were pre-warmed at 37˚C for 10 or 20 minutes, respectively. Cell suspension was loaded with FDG working solution, mixed and incubated at 37˚C for exactly one minute. The reaction was stopped by adding ice cold staining medium. Cells were analyzed and sorted immediately by FACS ARIA (Becton Dickinson) cell sorter. Gates were set following intensity of fluorescein signal and there were selected distinct positive and negative populations.

Recipient 4 week old athymic Nude-*Foxn1*^{nu} mice (Harlan Laboratories) were prepared by clearing the epithelium of the inguinal mammary glands on both sides to avoid interference from the host`s gland. Distinct fluorescein positive cells in limiting dilution series (10 000, 1000, 100) were implanted in 25 µl of BD Matrigel (BD Biosciences) on the one side and limiting serial dilution (10 000, 1000, 100) of distinct fluorescein negative cells on the other side as a control. The wound was closed using fine sutures. After 8 weeks restored mammary glands were dissected, spread on the glass slide and submerged in 2% paraformaldehyde in PBS for 3 hours. The mammary glands were then rehydrated in a series of ethanol dilutions (70%, 50%, 25%) and distilled water. Rehydrated glands were stained overnight in Carmine alum solution containing 1 g Carmine (C1022, Sigma), 2.5 g aluminium potassium sulphate (A7210, Sigma) per 500 ml of distilled water. Next, glands were dehydrated in a series of ethanol dilutions (70%, 95%, 100%) and bleached in xylenes for 48 hours. At the end mounted with Organo/Limonene Mount (O8015, Sigma). Samples were let dry overnight before imaging by light microscopy. Repopulating frequency and confidence intervals were calculated using limiting dilution analysis using Extreme Limiting Dilution Analysis (ELDA) software (http://bioinf.wehi.edu.au/software/elda/; (Hu and Smyth, 2009). ELDA uses a general linear model approach to calculate a maximum likelihood estimate from which the stem cell frequency is derived. Pairwise tests for differences in stem cell frequencies are determined by likelihood ratio tests using the asymptotic chi-square approximation to the log-ratio.

Mammary gland phenotype studies

Heterozygous and homozygous mice of B6.129P2-*AXL*^{tm1Dgen} strain (Jackson Labs) were sacrificed at 16 weeks, and mammary gland tissue harvested for Carmine alum whole-mount staining. Separate glands where harvested for formalin fixation and parafin embedded for subsequent H&E staining, immunofluorescence and IHC-P as described. Paraffin-embedded tissue sections from B6.129P2-*AXL*^{tm1Dgen} reporter mice were de-parafinized, antigen-retrieved (citrate buffer), and incubated 45 minutes in blocking buffer (5% goat serum in PBS w. 0.1% Triton X-100). Sections were then stained with primary antibodies chicken anti-beta galactosidase (1:100, ab9361, abcam), rat anti-Cytokeratin 8 (1:100, clone TROMA-1), and rabbit anti-Keratin 5 (1:400, PRB-160P-100, BioLegend) overnight at 4°C. To avoid cross-reactivity between the secondary antibodies, the samples were first incubated 45 minutes with AF647 goat anti-rabbit (1:200, A21244, Invitrogen) together with AF546 goat anti-rat (1:200, A11081, Invitrogen), then washed 3 times with PBS-T before a second round of 45 minutes incubation with AF488 rabbit anti-chicken IgY (IgG) Fc fragment specific (1:200, Jackson ImmunoResearch). Samples were then washed and mounted with ProLong Diamond Antifade Mountant with DAPI nuclear stain (P36962, Molecular Probes/Invitrogen) and imaged the next day with a Leica TCS Sp8 confocal microscope (Leica microsystems, Germany) using a 93x glycerin objective (NA = 1.3, WD = 0.30 mm, HC PL APO motCORR STED white). Images displayed in the figure are presented as a maximum projection of 4 z-stack images.

Warfarin treatment studies
12 week-old female C57BL/6 mice (UT Southwestern breeding core) were administered 1mg/L warfarin (Coumadin, Bristol-Myers Squibb Company) in drinking water. After five months of treatment mice were sacrificed and the mammary glands were dissected, fixed in 2% paraformaldehyde in PBS, stained with Carmine alum solution (Sigma C1022), cleared in xylene, mounted with Organo/Limonene (Sigma O8015) and imaged using brightfield tile scan with a Nikon TE2000. Treatment of pre-pubescent mice were initiated in 3 week old mice post-weaning. Mice were treated with either pure water or warfarin (1 mg/L) containing drinking water for 5 weeks prior to harvest of mammary glands and carmine alum staining as described above.

Generation of *MMTV-Wnt1:AXL+/+* and *MMTV-Wnt1:AXL$^{LacZ/LacZ}$* transgenic animals
MMTV-Wnt1 male mice (Jackson Laboratory) (Donehower et al., 1995; Tsukamoto et al., 1988) (kindly provided by Prof. Stein Ove Døskeland) were crossed with females of the *AXLLacZ* knock-in strain (B6.129P2-*AXL^{tm1Dgen}*, figure S5) to generate *MMTV-Wnt1*-positive females that develop spontaneous mammary tumors in a wildtype AXL$^{+/+}$ (*MMTV-Wnt1:AXL+/+)* and *AXL*-null (*MMTV-Wnt1:AXL$^{LacZ/LacZ}$*) background. Tumor formation was monitored by weekly palpation of the mammary glands from 1 month to 14 months of age. Previous studies showed that all *MMTV-Wnt1* females developed tumors within 1 year (Donehower et al., 1995, Tsukamoto et al., 1988). Mice that did not develop tumors within the duration of the 14-month observation period were scored as tumor-free.

Mammary tumor incidence studies
Female NOD/SCID *b2mnull* and Balb/c mice (6–8 weeks old; Gades Institute, University of Bergen) were used for tumor studies. The orthotopic 4T1-GFP-Luc mouse mammary carcinoma model was conducted as previously described (Gjerdrum et al., 2010). Cells were suspended in MEM/ EBSS medium/Matrigel (1: 1) (1x 10^6 cells in 50 µl) and were subsequently injected into the mammary fat pad of female BALB/c mice. Tumor growth were monitored and imaging of the ventral view were performed by the eXplore Optix Imaging System 10–15 min after D-luciferin (Biosynth) injection.

Xenograft tumor-initiation studies
Xenograft tumor-initiation studies were conducted as described by (Gupta et al., 2009). HMLER cells stably transduced by retroviral vectors (Slug, shLuc, shAXL) were suspended in DMEM/Matrigel (1:1) in a total volume of 50 µl and injected subcutaneously into the flank of NOD-SCID mice. Tumor incidence was monitored for up to 60 days after injection. For syngeneic tumor seeding studies, 4T1 cells were pretreated for 4 days with paclitaxel (3 nM) and bemcentinib (600 nM), and allowed to recover in the absence of drug for 1 week prior to injection. Tumor formation was assayed by palpation and caliper measurement between 7-9 days post implantation.

Histology and morphometry
The ductal morphology of mammary glands from 16 week old nulliparous *Axl$^{+/+}$* and*: Axl$^{LacZ/LacZ}$* of the B6.129P2-AXLtm1Dgen strain (The Jackson Laboratory, Bar Harbour, ME) mice were examined by hematoxylin/eosin (HE) stained FFPE tissue sections and carmine alum stained whole-mount specimens. Quantification of ductal area (µm2) per epithelial structure were performed on HE stained FFPE sections from *Axl$^{+/+}$* (n= 7) and *Axl$^{LacZ/LacZ}$* (n= 9) animals. Images were obtained using the NikonTE2000 microscope and area (µm2/ structure) were recorded using the Nikon software from 10 separate fields/ gland (Mann-Whitney p< 0.0001). Carmine alum stained mammary gland whole-mounts of 16-week old nulliparous *Axl$^{+/+}$* (n= 8) and *Axl$^{LacZ/LacZ}$* (n= 9) (B6.129P2-AXLtm1Dgen Strain, The Jackson Laboratory) mice were prepared and imaged as described. Both inguinal glands were included in the analysis. Ducts were partitioned from the background using image thresholding with MATLAB. The binary image obtained was sliced vertically pixel-wise. Segment lengths from the same duct were measured and averaged. FFPE sections from the mouse mammary fat pad tissue were stained by IHC-P for detection of ERalpha (ESR1) (ab37453, Abcam), Progesterone receptor (ab2765), and Ki67 (ab15580, Abcam). DAKO EnVisionTM System-HRP (DAB) for Rabbit primary antibodies (K4011, DAKO) were applied according to the manufacturer's instructions. Antibodies were diluted in antibody-diluent with

background reducing components (S3022, DAKO). Stained sections were counterstained with haematoxylin, prior to mounting using Faramount Aqueous Mounting Medium (S3225, DAKO). FFPE sections from the mouse mammary fat pad tissue were assessed for progesterone and estrogen receptor expression (scored strong or weak versus negative by trained pathologists), and proliferation rate by Ki-67 expression in luminal cells in the glands and duct structures. We used 25 high-power fields (x 400) and counted 20 luminal cells in each field (total of 500 luminal cells per case). Cells with cytoplasmic staining were not considered positive, and myoepithelial cells were not evaluated. All intensities of nuclear positivity were recorded as positive. The percentage of positive cells in each case was then calculated.

Statistical analysis

Where not otherwise stated, Graphpad Prism 5.0 for PC and Graphpad Prism 6.0 for Mac and MATLAB were used for statistical analysis using tests specified in the Figure Legends. The following symbols are shown to report established statistical significance: NS = $P > 0.05$, *$P \leq 0.05$, **$P \leq 0.01$, ***$P \leq 0.001$, ****$P \leq 0.0001$.

Supplemental references

AMIR EL, A. D., DAVIS, K. L., TADMOR, M. D., SIMONDS, E. F., LEVINE, J. H., BENDALL, S. C., SHENFELD, D. K., KRISHNASWAMY, S., NOLAN, G. P. & PE'ER, D. 2013. viSNE enables visualization of high dimensional single-cell data and reveals phenotypic heterogeneity of leukemia. *Nat Biotechnol,* 31**,** 545-52.

BODENMILLER, B., ZUNDER, E. R., FINCK, R., CHEN, T. J., SAVIG, E. S., BRUGGNER, R. V., SIMONDS, E. F., BENDALL, S. C., SACHS, K., KRUTZIK, P. O. & NOLAN, G. P. 2012. Multiplexed mass cytometry profiling of cellular states perturbed by small-molecule regulators. *Nat Biotechnol,* 30**,** 858-67.

CURTIS, C., SHAH, S. P., CHIN, S. F., TURASHVILI, G., RUEDA, O. M., DUNNING, M. J., SPEED, D., LYNCH, A. G., SAMARAJIWA, S., YUAN, Y., GRAF, S., HA, G., HAFFARI, G., BASHASHATI, A., RUSSELL, R., MCKINNEY, S., GROUP, M., LANGEROD, A., GREEN, A., PROVENZANO, E., WISHART, G., PINDER, S., WATSON, P., MARKOWETZ, F., MURPHY, L., ELLIS, I., PURUSHOTHAM, A., BORRESEN-DALE, A. L., BRENTON, J. D., TAVARE, S., CALDAS, C. & APARICIO, S. 2012. The genomic and transcriptomic architecture of 2,000 breast tumours reveals novel subgroups. *Nature,* 486**,** 346-52.

DONEHOWER, L. A., GODLEY, L. A., ALDAZ, C. M., PYLE, R., SHI, Y. P., PINKEL, D., GRAY, J., BRADLEY, A., MEDINA, D. & VARMUS, H. E. 1995. Deficiency of p53 accelerates mammary tumorigenesis in Wnt-1 transgenic mice and promotes chromosomal instability. *Genes Dev,* 9**,** 882-95.

DONTU, G., ABDALLAH, W. M., FOLEY, J. M., JACKSON, K. W., CLARKE, M. F., KAWAMURA, M. J. & WICHA, M. S. 2003. In vitro propagation and transcriptional profiling of human mammary stem/progenitor cells. *Genes Dev,* 17**,** 1253-70.

FELLENBERG, K., HAUSER, N. C., BRORS, B., NEUTZNER, A., HOHEISEL, J. D. & VINGRON, M. 2001. Correspondence analysis applied to microarray data. *Proc Natl Acad Sci U S A,* 98**,** 10781-6.

GJERDRUM, C., TIRON, C., HOIBY, T., STEFANSSON, I., HAUGEN, H., SANDAL, T., COLLETT, K., LI, S., MCCORMACK, E., GJERTSEN, B. T., MICKLEM, D. R., AKSLEN, L. A., GLACKIN, C. & LORENS, J. B. 2010. Axl is an essential epithelial-to-mesenchymal transition-induced regulator of breast cancer metastasis and patient survival. *Proc Natl Acad Sci U S A,* 107**,** 1124-9.

GUPTA, P. B., ONDER, T. T., JIANG, G., TAO, K., KUPERWASSER, C., WEINBERG, R. A. & LANDER, E. S. 2009. Identification of selective inhibitors of cancer stem cells by high-throughput screening. *Cell,* 138**,** 645-59.

HU, Y. & SMYTH, G. K. 2009. ELDA: extreme limiting dilution analysis for comparing depleted and enriched populations in stem cell and other assays. *J Immunol Methods,* 347**,** 70-8.

LABARGE, M. A., GARBE, J. C. & STAMPFER, M. R. 2013. Processing of human reduction mammoplasty and mastectomy tissues for cell culture. *J Vis Exp*.

LIM, E., VAILLANT, F., WU, D., FORREST, N. C., PAL, B., HART, A. H., ASSELIN-LABAT, M. L., GYORKI, D. E., WARD, T., PARTANEN, A., FELEPPA, F., HUSCHTSCHA, L. I., THORNE, H. J., FOX, S. B., YAN, M., FRENCH, J. D., BROWN, M. A., SMYTH, G. K., VISVADER, J. E. & LINDEMAN, G. J. 2009. Aberrant luminal progenitors as the candidate target population for basal tumor development in BRCA1 mutation carriers. *Nat Med,* 15**,** 907-13.

PELISSIER VATTER, F. A., SCHAPIRO, D., CHANG, H., BOROWSKY, A. D., LEE, J. K., PARVIN, B., STAMPFER, M. R., LABARGE, M. A., BODENMILLER, B. & LORENS, J. B. 2018. High-Dimensional Phenotyping Identifies Age-Emergent Cells in Human Mammary Epithelia. *Cell Rep,* 23**,** 1205-1219.

SUBRAMANIAN, A., TAMAYO, P., MOOTHA, V. K., MUKHERJEE, S., EBERT, B. L., GILLETTE, M. A., PAULOVICH, A., POMEROY, S. L., GOLUB, T. R., LANDER, E. S. & MESIROV, J. P. 2005. Gene set enrichment analysis: a knowledge-based approach for interpreting genome-wide expression profiles. *Proc Natl Acad Sci U S A,* 102**,** 15545-50.

SWIFT, S., LORENS, J., ACHACOSO, P. & NOLAN, G. P. 2001. Rapid production of retroviruses for efficient gene delivery to mammalian cells using 293T cell-based systems. *Curr Protoc Immunol,* Chapter 10**,** Unit 10 17C.

TAN, T. Z., MIOW, Q. H., MIKI, Y., NODA, T., MORI, S., HUANG, R. Y. & THIERY, J. P. 2014. Epithelial-mesenchymal transition spectrum quantification and its efficacy in deciphering survival and drug responses of cancer patients. *EMBO Mol Med,* 6**,** 1279-93.

TSUKAMOTO, A. S., GROSSCHEDL, R., GUZMAN, R. C., PARSLOW, T. & VARMUS, H. E. 1988. Expression of the int-1 gene in transgenic mice is associated with mammary gland hyperplasia and adenocarcinomas in male and female mice. *Cell,* 55**,** 619-25.

ZIVANOVIC, N., JACOBS, A. & BODENMILLER, B. 2014. A practical guide to multiplexed mass cytometry. *Curr Top Microbiol Immunol,* 377**,** 95-109.